INTERPRETING MULTIPLE SULFUR ISOTOPE SIGNALS IN MODERN ANOXIC SEDIMENTS USING A FULL DIAGENETIC MODEL (CALIFORNIA-MEXICO MARGIN: ALFONSO BASIN)

ANDREW MASTERSON*,†, MARC J. ALPERIN**, WILLIAM M. BERELSON***, and DAVID T. JOHNSTON*,†

ABSTRACT. Recent studies targeting the metabolic, physiological, and biochemical controls of sulfur isotope fractionation in microbial systems have drawn linkages between results from culture experiments and the sulfur isotope signatures observed in natural environments. Several of those studies have used newer techniques to explore the minor isotope (^{33}S and ^{36}S) variability in those systems, and also have attempted to place them in an ecophysiological context. Sparingly few have incorporated this newfound understanding of minor isotope behavior into natural systems (sediment pore waters, water columns) and none of them have refined existing isotope-dependent reaction-transport models to explicitly include ^{33}S. In this study, we construct a three-isotope (^{32}S, ^{33}S, and ^{34}S) reaction-transport model of pore water sulfate for a well-characterized sedimentary system within the California-Mexico Margin (Alfonso Basin). An additional goal is placing recent laboratory culture work into a natural, physical context. The model first reproduces the measured bulk geochemical characteristics of the pore water profiles of [SO_4^{2-}], [CH_4], dissolved inorganic carbon ([DIC]), and [Ca^{2+}]—and predicts bulk (non-isotope-specific but depth-dependent) rates of sulfate reduction. Next, the model uses those depth-dependent bulk rates, in combination with empirically calibrated fractionation factors, to explain the minor isotope characteristics ($\delta^{34}S$ and $\Delta^{33}S$ values) of the 0 to 40 cm pore water SO_4^{2-}. The down core, isotopic evolution of pore water sulfate requires a large fractionation associated with sulfate reduction ($^{34}\varepsilon_{SR} = 70 \pm 5‰$) that appears to be independent of bulk rate, but in line with low temperature thermody-namic predictions. The minor isotope characteristics ($^{33}\pm_{SR} \sim 0.5130$) are also independent of rate and fall within the range expected from microbial calibrations, but differ from minor isotope predictions of thermodynamic equilibrium. The high value of $^{34}\varepsilon_{SR}$ raises key questions in relating the physiological state of marine microorganisms relative to their laboratory counterparts, as well as point toward exceedingly low metabolic rates in natural marine sediments.

Key words: early diagenesis, sulfur isotopes, sulfate reduction, pore water sulfate

INTRODUCTION

Microbial sulfate reduction (MSR) is quantitatively the most important remineralization pathway for organic matter in modern continental margin sediments (Jorgensen, 1982) and carries profound geochemical consequences for the environmental interpretation of biogeochemical cycling (Canfield, 2004). Sulfur isotope geochemistry

* Department of Earth and Planetary Sciences, Harvard University, 20 Oxford St, Cambridge, Massachusetts 02138
** Marine Sciences Department, University of North Carolina, Chapel Hill, Chapel Hill, North Carolina 27599
*** Department of Earth Sciences, University of Southern California, Los Angeles, California 90089
† Corresponding authors: delmaistro@gmail.com or johnston@eps.harvard.edu

is a primary analytical tool for tracking and quantifying the influence of MSR and other sulfur metabolic pathways in those environments. Several decades of research focused on understanding the S isotope biochemistry of MSR (Rees, 1973; Detmers and others, 2001; Canfield, 2001) and metabolisms such as microbial sulfur disproportionation (Bak and Pfenning, 1987; Canfield and Thamdrup, 1994; Thamdrup and others, 1994; Canfield and Teske, 1996; Finster and others, 1998; Habicht and others, 1998). Those studies targeted the two most abundant sulfur isotopes ($^{34}S/^{32}S$) and largely used the magnitude of a fractionation ($^{34}\varepsilon$, see definition below) as a diagnostic feature for distinguishing between different metabolisms.

In natural marine seafloor environments, where MSR flourishes, diagenetic reaction transport modeling complements isotopic studies and is the primary means for reconstructing microbial reaction rates from the concentrations of pore water and solid phase species. The mathematical framework underlying the modeling has long been established (Berner, 1980; Boudreau, 1997) and models of increasing complexity are continuing to be constructed (compare Arndt and others, 2013). Such models have been used to understand organic matter degradation kinetics (Aller, 2014), methane biogeochemistry (for example, Alperin and others, 1994), and as explored further here, sulfur cycling (Berner, 1964; Jorgensen, 1979; Aller and Blair, 1996; Aller and others, 2010). Sometimes bulk geochemical rates serve as model inputs, but more often biogeochemical rates, derived from concentration profiles, are the desired model output (Bowles and others, 2014). A small cadre of studies have constructed such models for understanding measured S isotope profiles in sulfate and sulfide, beginning with the seminal study of Jorgensen (1979), and later to more unique localities like the deep biosphere (Wortmann and others, 2001) and Cariaco Basin (Donahue and others, 2008). As with the aforementioned microbial work, these efforts employed measurements and modeling of the conventional $^{34}S/^{32}S$ values in the target sulfur bearing phases.

With the application of multiple or *minor* sulfur isotope systematics (specifically $^{33}S/^{32}S$ and $^{36}S/^{32}S$) to microbial systems, researchers expanded the utility of isotope studies as an informant of microbial process (Farquhar and others, 2003). The small, but analytically resolvable kinetic isotope fractionations generated by microbial processes remain a target of much new research (Leavitt and other, 2013), the underpinning of which is firmly rooted in the physical chemistry of mass-dependent isotope fractionation (Bigeleisen and Mayer, 1947; Young and others, 2002; Farquhar and others, 2003). These emerging studies of biological systems highlight the added level of interpretability that comes with exploring related triple isotope metrics (here $\delta^{34}S$, $\Delta^{33}S$, and $^{33}\lambda_{SR}$ - the rigorous definition of these different metrics is provided below).

Early applications of $^{33}S/^{32}S$ measurements, paired with an understanding of how mass is conserved at the cellular scale, demonstrated that the signatures of MSR and sulfur disproportionation are distinguishable and unique (Johnston and others, 2005a; Johnston and others, 2005b; Johnston and others, 2008). This is in contrast to simply using the classic $^{34}S/^{32}S$ measure (Canfield, 2001). This discovery led to minor S isotopes being used to understand S cycling and the antiquity of different processes within ancient systems (Johnston and others, 2005a; Johnston and others, 2005b; Johnston and others, 2008). Subsequent studies have further characterized multiple S isotope signatures in microbial experiments (Johnston and others, 2007; Sim and others, 2011; Sim and others 2012) and improved our understanding of the influence of rate (Leavitt and others, 2013), sulfate concentration (Bradley and others, 2015), and enzyme effects (Leavitt and others, 2015) in the ultimate expression of multiple S isotope biosignatures. Due to the overwhelming importance of MSR in the historical S isotope record (for example, Strauss, 1999), multiple S isotope studies have also tried to interpret these mass-dependent $^{33}S/^{32}S$ signatures in proxy records (Johnston and

others, 2008; Wu and others, 2010; Wu and others, 2015; Sim and others, 2015; Masterson and others, 2016). The variability in the $^{33}S/^{32}S$ record is clearly connected to microbial metabolism, but the proper quantification of the connection between laboratory calibrations of microbial signatures depends on placing those isotopic observations into a diagenetic context; recall that most geologic sedimentary records began their life as marine sediments. In keeping with approaches to the $^{34}S/^{32}S$ system (compare Jorgensen, 1982), only one study has extended a diagenetic model to include the multiple S isotopes. Here, Pellerin and others (2015) constructed a diagenetic model to describe a pore water sulfate concentration profile and associated isotope information from Mangrove Lake, Bermuda. Fortunately, information from allied elemental and isotopic systems (see C, Fe, N, *et cetera*) provides added leverage on the behavior of the sulfur cycle in these settings. The natural extension of previous work is then to interpret sulfate concentration profiles in parallel with those of other geochemical species (organic matter, CH_4, DIC) in order to improve the quantification of biogeochemically important rates (such as sulfate reduction and anaerobic methane oxidation). In concert with multiple S isotope information, this next generation of model will allow for a better understanding of the connection between laboratory studies of microbial signatures—where rates are generally well understood—and natural systems.

In this study, we use pore water data and samples from an anoxic basin in the Baja California-Mexico margin, Alfonso Basin, to reconstruct sedimentary S cycling and to understand the implications for interpreting minor S isotope ($\Delta^{33}S_{SO4}$) pore water sulfate profiles. The anoxic-silled basins of the California-Mexico margin are an ideal place to study S cycling due to their low bottom water O_2 content (<5 μM), laminated sediments, and high particulate organic carbon (POC) content ($>5\%$). Alfonso Basin in particular has been well-studied (Berelson and others, 2005; Gonzalez-Yajimovich and others, 2007; Staines-Urias and others, 2015). Sediment and pore water data previously sampled and measured (Berelson and others, 2005) during the CalMex campaign of 2001 from which tour samples include POC, $[SO_4^{2}]$, $[CH_4]$, [DIC], and $[Ca^{2+}]$, and form the basis for our model. The model includes organic matter degradation kinetics, sulfate reduction, methanogenesis, anaerobic methane oxidation, and authigenic carbonate precipitation. The essential output of that bulk model is a *net* sulfate reduction rate (SRR) that is used as a model input for running an isotope-specific reaction transport model for the isotopologues of interest ($^{32}SO_4^{2-}$, $^{33}SO_4^{2-}$, $^{34}SO_4^{2-}$, and where ^{33}S is less than 1% of total sulfur). We ignore $^{36}SO_4^{2-}$ because of its very low abundance ($<0.02\%$). The model inputs include fractionation factors associated with sulfate reduction—$^{33}\alpha_{SR}$ and $^{34}\alpha_{SR}$—and the model outputs include pore water sulfate $\delta^{34}S$ and $\Delta^{33}S$ profiles. The results demonstrate that it is possible to extract intrinsic S isotope fractionation behavior from a sediment column, and to use pore water $\Delta^{33}S$ and $\delta^{34}S$ profiles to extrapolate microbial calibrations to natural environments where biogeochemical rates are largely unconstrained.

ISOTOPE NOMENCLATURE

Multiple isotope systems require an expanded set of notation to fully capture the witnessed and calculated variability. The common nomenclature used to define the standard $^{34}S/^{32}S$ ratios is simply delta notation, relating a sample and a standard (VCDT):

$$\delta^{34}S = 1000 \cdot \left[\frac{(^{34}S/^{32}S)_{samp}}{(^{34}S/^{32}S)_{VCDT}} - 1 \right]. \quad (1)$$

The difference between two measured $\delta^{34}S$ values can also be captured as $^{34}\varepsilon$. For example, the difference between the composition of sulfate ($\delta^{34}S_{sulfate}$) and sulfide

($\delta^{34}S_{sulfide}$) would be represented as ${}^{34}\varepsilon_{sulfate\text{-}sulfide} = \{[(\delta^{34}S_{sulfate}/1000 > 1)/(\delta^{34}S_{sulfide}/1000 > 1)] > 1\} * 1000$ or $[{}^{34}\alpha > 1] * 1000$. Here, we also use a classic definition of α, which is a fractionation factor and equal to the ratio of ratios. As all the effects described herein are mass-dependent (Johnston, 2011), they are small and difficult to interpret as $\delta^{33}S$ (all ^{33}S nomenclature holds equally for ^{36}S). As a result, it is now commonplace to normalize data to an 'expected' mass-dependent reference line, with a slope of 0.515 when relating $\delta^{33}S$ to $\delta^{34}S$. This reference value approximates thermodynamic equilibrium (Farquhar and others, 2003). This results in a Δ notation, which is the deviation from that reference line in units of parts per thousand (or ‰):

$$\Delta^{33}S = \delta^{33}S - 1000 \cdot \left[\left[\frac{\delta^{34}S}{1000} + 1\right]^{0.515} - 1\right]. \quad (2)$$

In cases where non-equilibrium fractionations or physical processes like mixing are involved, it is convenient to introduce another term, ${}^{33}\lambda$, which is effectively a line that connects two distinct isotopic compositions (for instance a reactant and product relationship like sulfate and sulfide). This is a line that commonly only deviates in slope/value from the reference line by less than 1 percent and is more rigorously defined as:

$${}^{33}\lambda = \frac{ln({}^{33}\alpha)}{ln({}^{34}\alpha)} \quad (3)$$

for the $^{33}S/^{32}S$ and $^{34}S/^{32}S$ system. In practice, the ${}^{33}\lambda$ term can simply be seen as another measure of a minor sulfur isotope fractionation and will vary around a value of 0.515.

ALFONSO BASIN SAMPLING AND ENSUING ANALYTICAL METHODS

Coring and pore water sampling of Alfonso Basin took place during the CalMex cruise of October and November 2001. That particular sampling cruise processed sediment cores from numerous sites along the California and Mexican margin (Berelson and others, 2005). We have focused on Alfonso Basin and briefly describe the sample site characteristics and pore water sampling protocols. Although there is some temporal variability, in general, bottom water oxygen concentrations are less than 5 μM, and sediments are laminated, indicating long-term bottom water anoxia. Alfonso Basin, station 15 (24° 38.18', 110° 36.06) lies off the coast of La Paz (Baja Mexico) and was sampled at a water depth of 408 m (see fig. 1). Coring was done with a multicorer and a gravity corer. Cores with a well-preserved sediment-water interface were utilized for whole-core squeezing to extract pore waters to define gradients in the upper few centimeters. Additional multicores from each station were sectioned in an anoxic glove bag. Sections were alternatingly sampled for methane (CH_4) and dissolved SO_4^{2-}, Ca^{2+}, DIC, NH_4^+, and silica. Methane was sampled and analyzed as described in Sansone and others (2004), as revisited in Berelson and others (2005). Pore water was filtered and stored in glass syringes for DIC analysis and bottled for the remaining constituents. See Appendix for all pore water data, in addition to sulfur isotope data generated in this study.

Frozen, unacidified pore waters from the CalMex (2001) cruise were shipped to the laboratory for Stable Isotope Geobiology at Harvard University in 2014 for further sample preparation and isotope analyses. Thawed pore water samples were acidified with 1N HCl to a pH of ~2.5, and to each sample (ranging in volume from 0.25 mL – 3.0 mL) 500 μL of a concentrated solution of barium chloride (1M $BaCl_2$) was added in order to precipitate sulfate as $BaSO_4$. Barium sulfate precipitates were rinsed several times with deionized water and dried for a minimum of 12 hours for $\delta^{34}S_{SO4}$ analyses.

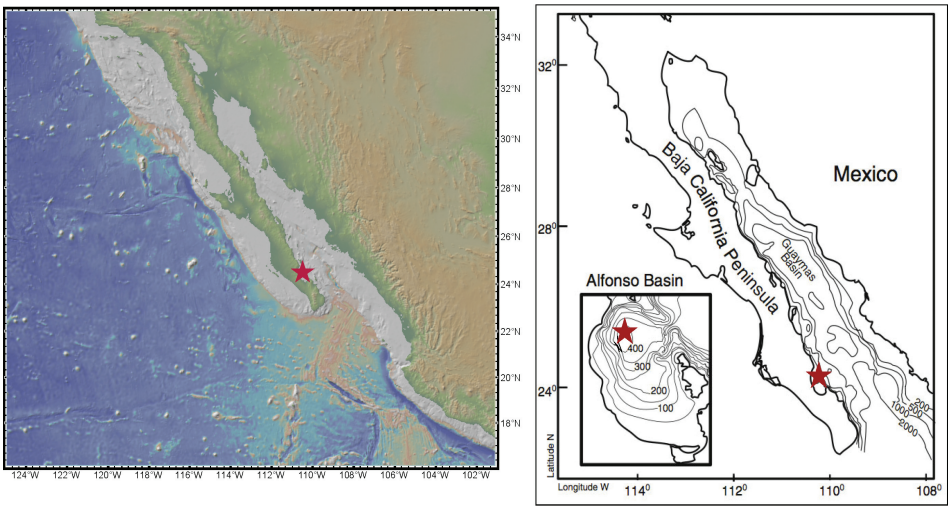

Fig. 1. Map showing the sampling locality within Alfonso Basin for the cores studied herein. The cores were sampled at approximately 408 m water column depth, at latitude of 24°38.18' (N) and longitude of 110°36.06' (W) in November 2001. Separate cores (multi cores and gravity cores) were retrieved, and archived sulfate provided the material for analysis in this study. The details of the cruise, and the sampling were originally published in Berelson and others (2005). The left panel provides the location of Alfonso Basin, and the right panel, a modified version of that appearing in Staines-Urias and others (2015), provides the details of the bathymetry of the California-Mexico margin.

Isotope analyses for $\delta^{34}S_{SO4}$ were done directly on $BaSO_4$ precipitates using continuous flow IRMS where SO_2 is the analyte gas. Here, online combustion utilizing a V_2O_5 catalyst at 500 °C was performed with a Costech EA, mated to the Delta V. Reproducibility was estimated from repeat analyses of IAEA-S-1, S-2, S-3, as well as NBS-127, to be better than ±0.2 permil (1σ).

For minor isotope measurements ($\delta^{33}S_{SO4}$), samples were first chemically converted to Ag_2S by reductive distillation with a mixture of hydriodic acid (HI), hypophosphorous (H_3PO_2) and hydrochloric acid (HCl) at ~90 °C for 3 hours (Forrest and Newman, 1977). The reactors were purged with N_2 and product H_2S was captured as ZnS and converted to Ag_2S by cation exchange with $AgNO_3$. Samples were rinsed with ~100 mL of Millipore water, 15 mL of 1M NH_4OH, an additional ~100 mL of Millipore water, and dried in a 90 °C oven overnight. Powdered Ag_2S samples were fluorinated at 300 °C in a F_2 atmosphere at 10X stoichiometric excess. Product SF_6 was cryogenically and chromatographically purified and analyzed on a Thermo Finnigan 253 in Dual Inlet mode. Analyses of repeat standards of IAEA-S-1, S-2, S-3, yield a reproducibility of ±0.2 permil and ±0.006 permil for $\delta^{34}S$ and $\Delta^{33}S$, respectively. Samples are reported versus VCDT, calibrated from the long-term running average of IAEA-S-1 versus the working standard gas at Harvard University (see Johnston and others, 2014 for a full minor isotope calibration of these standards).

MODEL CONSTRUCTION

All reaction-transport models used in this study are steady-state finite-difference models, and were coded and run in Fortran 77 to a specified depth (that is, model domain length, L; Alperin and others, 1999). The baseline geochemical model that reproduces the bulk pore water profiles consists of two parts: (1) an organic carbon degradation model that produces a depth profile of remineralization rates (GRR), and (2) a reaction-transport model that calculates depth-dependent reaction rates, such as

TABLE 1

Upper boundary conditions of the baseline geochemical model

Solute	Concentration (mmol/L)	Source
SO_4^{2-}	28.93	I†
CH_4	0.00025	L[1]
DIC	2.35	L[2]
Ca^{2+}	10.53	I†
Solid	**Concentration (%)**	**Source**
POC	7.79	L[3]
POC_∞	2.24	C
G	5.55	C
Solid	**Flux (mmol cm^{-2} y^{-1})**	**Source**
G_1	0.990	C
G_2	4.170	C
G_3	4.760	C

Solid phase and pore water concentration boundary conditions for the baseline geochemical model. In this table and the remaining tables, the Source terms refer to L = Literature, I = calculated from other model conditions (described in text), and C = Model variable/parameterization.

† Determined from a salinity of S = 35.

[1] Sansone and others (2004).

[2] Berelson and others (2005).

[3] Silverberg and others (2014).

organoclastic sulfate reduction, methanogenesis, and anaerobic methane oxidation. The model also solves for boundary values and the final output reproduces the measured pore water profiles of [SO_4^{2-}], [CH_4], DIC, and [Ca^{2+}]. A key output of the model is the depth-dependent rate profiles, such as sulfate reduction rate (SRR) and anaerobic methane oxidation rate. The output SRR, in concert with the upper [SO_4^{2-}] boundary conditions and isotope information is then used to run the isotope-specific reaction transport model that computes independent rates (^{32}SRR, ^{33}SRR, and ^{34}SRR), as well as isotope profiles ($\delta^{34}S$ and $\Delta^{33}S$) that can be used to fit the measured data. Discussed below are the more explicit details of the model construction (boundary conditions, diffusion coefficients, kinetics parameters) that were used to run each of the models. Further derivation and details are provided in the Appendix, as the main text provided below targets only the essential details of this application.

There are a number of physical parameters that are critical to the analysis. For instance, model inputs for the baseline simulation are physical parameters such as the size of the model domain (L = 300 cm) below which compaction is negligible. Water depth, z = 408 m, temperature, T = 9 °C, and salinity, S = 35 were all specified and are used to compute the diffusion coefficients, which are influenced by the physical chemical characteristics of seawater (see tables 2 and 3). Dry sediment density, ρ_{SM} = 2.65 g/cm^3 and the mass accumulation rate F_{SM} = 0.0149 g/cm^2 are also necessary to properly compute the coefficients in the diffusion and advection terms of the reaction-transport equations. Mass accumulation rate is critical in determining the flux of POC into the model domain since it parameterized as a weight percent of carbon in total solids. Porosity (ϕ), or the fraction of whole sediment volume occupied by pore water, was measured at the time of pore water sampling of the multi- and gravity cores. The porosity profile follows a characteristic, exponential decay function with steady-state

TABLE 2

Physical parameters used in the baseline model

Symbol	Description	Value	Units	Source
z	Water depth	408	m	L[1]
T	Bottom water temperature	9	°C	L[2]
S	Bottom water salinity	35	psu	L[1]
L	Length of model domain	3000	cm	C
φ_o	Porosity at sediment surface	0.945	-	C
φ_∞	Porosity below zone of compaction	0.835	-	C
β	Porosity attenuation coefficient	0.0147	cm^{-1}	C
ρ_{SM}	Dry sediment density	2.65	$g\ cm^{-3}$	L[1]
F_{SM}	Mass accumulation rate	14.9	$mg\ cm^{-2}\ y^{-1}$	L[1]

[1] Gonzalez-Yajimovich and others (2007).
[2] Berelson and others (2005).

compaction (see fig. 2A). That is, it is allowed to vary with depth and is not held constant. This model fit is used throughout the reaction-transport equations.

The boundary conditions were calculated using salinity data from an adjacent study (Gonzalez-Yajimovich and others, 2007). From this, it was determined that the upper boundary concentration conditions for $[SO_4^{2-}]$ at 28.93 mM and $[Ca^{2+}]$ at 10.2 mM. The upper boundary conditions for $[CH_4]$ and DIC were as determined in Sansone and others (2004). In all model runs, the upper boundary conditions for the five species were constant (Dirichlet) concentrations (for example, [C]), and the lower boundaries were Neumann ($d[C]/dx = 0$) gradients. Boundary conditions for all species used in the baseline geochemical model, including POC, and described in more detail below, are shown in table 1.

Organic carbon remineralization is parameterized using a classic '3G' model (Westrich and Berner, 1984; Dale and others, 2009). In this formulation, particulate organic carbon (POC) deposited at the sediment water interface (that is the boundary condition) is divided into four fractions: an unreactive fraction, the concentration of which remains constant throughout the model domain (POC_∞), and three fractions

TABLE 3

Diffusion coefficients of aqueous species (cm^2/s)

	25°C, 0 psu, 0 m [(1)]	9°C, 35 psu, 408 m [(2)]
D_{SO4}	$10.7x10^{-6}$	$6.5x10^{-6}$
D_{CH4}	$16.7x10^{-6}$	$10.1x10^{-6}$
D_{DIC}	CO_2: $19.7x10^{-6}$	CO_2: $11.7x10^{-6}$ ($\alpha_o = 2.92\%$)[3]
	HCO_3^-: $11.9x10^{-6}$	HCO_3^-: $7.23x10^{-6}$ ($\alpha_1 = 95.26\%$)[3]
	CO_3^{2-}: $9.31x10^{-6}$	CO_3^{2-}: $5.65x10^{-6}$ ($\alpha_2 = 1.82\%$)[3]
		DIC: $7.33x10^{-6}$[4]
D_{Ca}	$8.08x10^{-6}$	$4.91x10^{-6}$

[1] Boudreau (1997).
[2] Corrected to in situ temperature, salinity, and pressure used in the Stokes-Einstein equation.
[3] α values calculated at *in situ* temperature, salinity, and pressure (assumed pH 7.5) using csys (Zeebe and Wolf-Gladrow, 2001).
[4] $D_{DIC} = \alpha_o D_{CO2} + \alpha_1 D_{HCO3} + \alpha_2 D_{CO3}$.

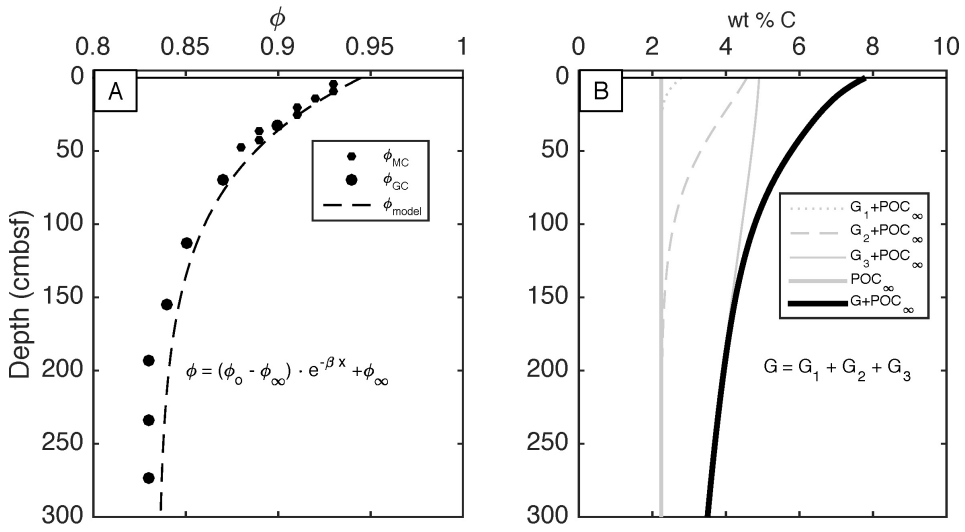

Fig. 2. (A) Porosity (ϕ) data from the gravity (GC) and multicores (MC) used in this study, and originally published in Berelson and others (2005). The exponential fit to the porosity data is typical of continental margin sediments and is used to determine the porosity in the diagenetic models constructed here. (B) Model parameterization of organic carbon degradation kinetics. The '3G' model used here partitions the pool of reactive carbon (G) into three fractions with shared reactivity (G_1, G_2, G_3), where $k_1 > k_2 > k_3$. The respective sizes of the pools G_n are adjustable, as are the rate constants. POC_∞ is the fraction of organic matter completely resistant to degradation, and $G+POC_\infty$ implies the size (wt% C) of total organic carbon within the Alfonso Basin sediments. In all sediment profile figures, the solid line at depth = 0 is the sediment water interface.

(G_1, G_2, and G_3) with decreasing reactivity towards remineralization. The relative contributions of each fraction to the total reactive carbon pool are adjustable as model inputs. The solution to the 3G model was solved assuming first order decay for each fraction of G, and the remineralization rate normalized to reflect the pore water concentration of C remineralized. Thus, GRR_{pw} is determined in units of μmol/cm^{3}d. A more detailed description of GRR is provided in Appendix 1. In keeping with this approach, the remineralization rate constants ($k_1 > k_2 > k_3$) are adjustable as model inputs with the chosen values presented in tables 1 and 4. As elaborated upon in previous studies that apply the same approach (Dale and others, 2009), the reactive fractions G_n do not resemble actual carbon compounds, but are a simplified means of modulating the rate kinetics of the whole model. Since all other rates (including SRR and AOM) are calculated from GRR, the concentration profiles are most easily adjusted by changing the fraction of each G_n and their respective remineralization rate constants.

Now closing in on sulfate reduction, the bulk model assumes that organic carbon is degraded via only two pathways: organoclastic sulfate reduction and methanogenesis. Thus, aerobic oxidation, which is minimal in a basin like Alfonso, is neglected. Dissimilatory Fe reduction is also excluded. Quantifying the sulfate reduction rate, SRR, with respect to GRR requires knowledge of the oxidation state of organic matter (XS) as it influences the stoichiometry of remineralization (C/S). Moreover, the mathematical constraints of the diagenetic model require parameterizing sulfate limitation (to dampen rates at low sulfate thresholds) for SRR, and require a similar parameterization of sulfate inhibition for methanogenesis. These are accomplished with the error function (erfc) – a smoothed version of a step function that dials down rates when sulfate concentrations reach the threshold ($[SO_4^{2-}]^*$) of limitation and

TABLE 4

Kinetic and equilibrium parameters of baseline model

Parameter	Description	Value	Unit	Source
k_1	Reactivity of POC pool G_1	0.0100	y^{-1}	C
k_2	Reactivity of POC pool G_2	0.0010	y^{-1}	C
k_3	Reactivity of POC pool G_3	0.0001	y^{-1}	C
f_1	Fraction of reactive POC pool as G_1	0.100	-	C
f_2	Fraction of reactive POC pool as G_2	0.420	-	C
k_{MO}	Rate constant for methane oxidation	0.250	yr^{-1}	C
$[SO_4^{2-}]^*$	Threshold concentration for sulfate uptake	0.200	mM	L[1]
k_{CaCO3}	Rate constant for calcite precipitation	0.030	mM y^{-1}	L
K_{ADS}	Equilibrium adsorption coefficient for Ca^{2+}	1.6	$cm^3\ g^{-1}$	L[2]
$K'_{sp,calcite}$	Solubility product for calcite	4.92×10^{-7}	M^2	L[3]
XS	Oxidation state of organic matter	-0.7		L[4]

[1] Habicht and others (2002).
[2] Li and Gregory (1974).
[3] Zeebe and Wolf-Gladrow (2001).
[4] Alperin and others (1994).

inhibition. Here the thresholds are shared for both limitation (in the case of sulfate reduction) and inhibition (in the case of methanogenesis), and is prescribed as $[SO_4^{2-}]^* = 200\ \mu M$. That limit is one of several estimated from sulfate affinity measurements (Tarpgaard and others, 2011) and also from isotope fractionation studies of MSR in culture (Habicht and others, 2002). The incorporation of this parameterization into the reaction terms is detailed more clearly in Appendix 1, but the most important consequence of this input is to prevent the occurrence of *negative* rates [mathematically feasible, but entirely unphysical, and a classical problem in early diagenetic modeling (Boudreau and Westrich, 1984; Boudreau, 1997)]. Rate constants also appearing in the model (see table 4) are that for anaerobic methane oxidation (k_{AOM}) and the kinetic and equilibrium constants associated with $CaCO_3$ precipitation and Ca^{2+} adsorption.

To have a more realistic and complete carbon cycle, we include dissolved inorganic carbon and $CaCO_3$ precipitation in the model. DIC production rates are directly linked to GRR and methane oxidation, and the $CaCO_3$ precipitation rate is expressed as a function of the saturation state of $CaCO_3$. Here we assume constant pore water pH value of 7.5, similar to that observed in the Santa Barbara Basin (Riemers and others, 1996). Carbonate precipitation is then proportional to the degree of supersaturation (for example, $\Omega = [Ca^{2+}][CO_3^{2-}]/K'_{carb}$). Since a substantial fraction of DIC and pore water Ca^{2+} is lost to $CaCO_3$, including these rates is necessary to reproduce the DIC and $[Ca^{2+}]$ pore water profiles and can be used as a feasibility check on DIC production via GRR and methane oxidation. Note that the carbon cycle is here included for completeness and has no direct bearing on sulfur isotope predictions.

The sum of the discussion above is the extraction of a sulfate reduction rate. Importantly, the SRR included sulfate consumed via organoclastic sulfate reduction and via methane oxidation. While it is theoretically possible to calculate the *isotope-specific* rates of sulfate reduction (^{32}SRR, ^{33}SRR, and ^{34}SRR) and incorporate them into the same model, it is far more straightforward to use the output *bulk* sulfate reduction rates, by definition SRR = ^{32}SRR + ^{33}SRR + ^{34}SRR, as the model input for a separate

TABLE 5

Values used for upper boundary condition calculation in $^{32}SO_4^{2-}$, $^{33}SO_4^{2-}$, $^{34}SO_4^{2-}$ isotope model

	Value	Units	Source
Solute			
SO_4^{2-}	28.93	mM	L[1]
Composition			
$\delta^{34}S$	21.150	‰	L[2]
$\Delta^{33}S$	0.0475	‰	L[2]
Ratio			
$^{33}R_{VCDT}$	0.00787726	-	L[3]
$^{34}R_{VCDT}$	0.04416264	-	L[3]
Species			
$^{32}SO_4^{2-}$	27.472	mM	C[4]
$^{33}SO_4^{2-}$	0.218	mM	C[4]
$^{34}SO_4^{2-}$	1.239	mM	C[4]

[1] Gonzalez-Yajimovich (2007).
[2] Johnston and others (2014).
[3] Coplen and others (2002).
[4] Calculations are shown in Appendix 2.

isotope model that considers only the sulfate isotopologues $^{32}SO_4^{2-}$, $^{33}SO_4^{2-}$, and $^{34}SO_4^{2-}$.

ISOTOPIC MODEL COMPONENTS

One clear novelty of this work is the extension of a prior diagenetic model framework to include the triple sulfur isotope system. Researchers have previously approached the problem of calculating isotope-specific rates from the total rate, both for sulfur (Jorgensen, 1979) and carbon (Alperin and Hoehler, 2009). As expected, it requires (i) the natural abundance ratio of the two or more isotopes in a known material, usually a standard, (ii) knowledge of the isotopic composition of the starting reservoir or boundary condition, and (iii) the fractionation factors (α) for the particular microbial processes involved, in order to calculate their abundance as a reaction proceeds. The formulation is fairly simple for two isotope systems, but algebraically more complex with three or more isotopes. For this study, the derivation of the isotope-specific boundary conditions for [$^{32}SO_4^{2-}$], [$^{33}SO_4^{2-}$], and [$^{34}SO_4^{2-}$], as functions of $\delta^{34}S$ and $\Delta^{33}S$ values, as well as the isotope-specific reaction terms with respect to SRR and the fractionation factors ($^{34}\alpha_{SR}$ and $^{33}\alpha_{SR}$) are shown in Appendix 2. The actual concentrations of $^{32}SO_4^{2-}$, $^{33}SO_4^{2-}$, and $^{34}SO_4^{2-}$, which are used as upper boundary conditions in the isotope model, are shown in table 5. As in the baseline geochemical model, all lower boundary conditions for the isotope model are Neumann conditions (that is, determined by the rate of change rather than an absolute value).

As with other S isotope reaction-transport models ($^{34}S/^{32}S$, Jorgensen, 1979; Dale and others, 2009; Aller and others, 2010), the input fractionation factors are an important component of quantifying the rates for individual species (^{32}SRR, ^{33}SRR,

^{34}SRR) with respect to bulk rate. Put differently, the fractionation factors are the ratio of isotope-specific rate constants for a particular biogeochemical process. In the case of each isotope model run, the input values include fractionation factors, $^{34}\alpha_{SR}$ and $^{33}\alpha_{SR}$. In keeping with previous determinations (compare Young and others, 2002), the $^{33}\alpha_{SR}$ is calculated using a term $^{33}\lambda_{SR}$, where:

$$^{33}\alpha_{SR} = (^{34}\alpha_{SR})^{^{33}\lambda_{SR}}. \quad (4)$$

The computation of the individual rates for ^{32}SRR, ^{33}SRR, and ^{34}SRR is shown in Appendix 2. There we demonstrate how the accurate determination of each depends on SRR, [$^{32}SO_4^{2-}$], [$^{33}SO_4^{2-}$], [$^{34}SO_4^{2-}$], $^{33}\alpha_{SR}$, and $^{34}\alpha_{SR}$. The isotope-specific diagenetic model considers all species independently, but they are mathematically linked through their reaction terms.

The model output produces depth-dependent concentrations of [$^{32}SO_4^{2-}$], [$^{33}SO_4^{2-}$] and [$^{34}SO_4^{2-}$], which are used to calculate the isotope profiles of $\delta^{34}S_{SO4}$ and $\delta^{33}S_{SO4}$. These values are then used in conjunction with equation 2 to calculate $\Delta^{33}S_{SO4}$. Although the bulk sulfate reduction rates are fixed, the sulfate isotopologue profiles are adjustable with $^{34}\alpha_{SR}$ and $^{33}\lambda_{SR}$. These values ($^{34}\alpha_{SR}$ and $^{33}\lambda_{SR}$), which in the case of the model can vary and are chosen to fit the measured sulfate isotope profiles, are then comparable to the fractionations extracted from laboratory studies with sulfate reducing bacteria and archaea.

RESULTS AND DISCUSSION

Sediment Geochemistry Profiles and Rates

As organic carbon is the key electron donor for sulfate reduction, we begin with considering this component of the system. Gonzalez-Yajimovich (ms, 2004) quantified the weight percent of the top 10 cm of Alfonso Basin sediments using the same New Horizon cores employed for this study and found POC = 6.2 ± 0.4 weight percent, with the largest values measured at 6.85 percent (table 1). At 250 to 300 cm, POC values have decreased to 3.3 ± 0.2 percent, consistent with other studies (Berelson and others, 2005). However, as suggested in Gonzalez-Yajimovich and others (2007), there is evidence of seismically induced turbidity flow in Alfonso Basin, leading to non-steady state conditions of sedimentation deeper in the core. This is consistent with Alfonso being a small marginal basin in the tectonically active Gulf of California. Despite this evidence for non-steady conditions, a simple linear loss model ($r^2 = 0.8$) for organic carbon implies ~1.0 weight percent loss per 100 cm for the top 300 cm (see also Berelson and others, 2005). The POC modeled in the reaction transport model (3G model) overestimates the concentration at shallow depths (POC_o = 7.79%), but accurately reproduces the concentrations mid-depth. The upper boundary condition was derived from estimates of sinking POC fluxes from sediment trap data in Alfonso Basin (Silverberg and others, 2014).

From here, the 3G model partitioned the 'reactive' organic matter into three different fractions, lumped by reactivity. Each fraction decays (independent mathematically) with first-order decay kinetics with decay constants k_1, k_2, and k_3 for G_1, G_2, and G_3, respectively. The values used for the first-order decay constants ($k_1 = 0.0100\ yr^{-1}$, $k_2 = 0.0010\ yr^{-1}$, and $k_3 = 0.0001\ yr^{-1}$) were chosen to fit the data, as were the respective fractions of G (f_1, f_2, $f_3 = 1 - f_1 - f_2$). The weight percent of each fraction is displayed in figure 2B, as is total weight percent POC. It is worth noting that G_1 and G_2 are consumed almost entirely by organoclastic sulfate reduction, and that a substantial fraction of G_3, the least reactive fraction of G, is lost via methanogenesis. The summed remineralization rates of the fractions G leads to GRR_{PW}, which decreases from ~2 $\mu mol/cm^3\ d^{-1}$ at the sediment water interface to ~0 at the lower boundary (fig. 3). The output rates for the rest of the model, including SRR, are mathematically linked to

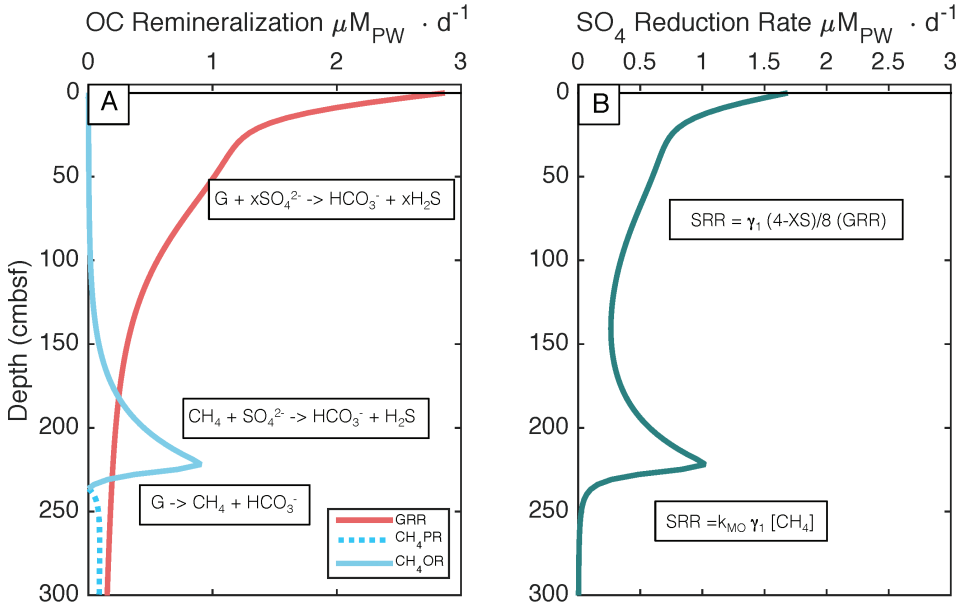

Fig. 3. (A) Model output from the 3G POC degradation model that parameterizes the remineralization rate, GRR (μM_{PW} d^{-1}), the methane production rate CH_4PR, and the methane oxidation rate CH_4OR. The rates are the primary output of the 3G model, and are used to determine the sulfate reduction rate. (B) Modeled sulfate reduction rate, SRR (μM_{PW} d^{-1}), determined from the organic carbon remineralization and methane oxidation rates, as shown in (A). The different stoichiometries of oxidation 1:1 in the case of methane oxidation, and related to the oxidation state of organic matter, XS, in the case of GRR control their contribution to SRR. In all cases, sulfate consumption is reduced in cases where sulfate is limiting ($[SO_4^{2-}] < [SO_4^{2-}]^*$).

GRR via the reaction stoichiometry of the process of interest. Since there is no direct proxy for remineralization rates, the kinetics were tuned by the $[SO_4^{2-}]$ and $[CH_4]$ profiles.

The pore water sulfate concentration data in Alfonso Basin exhibits a near linear profile (Berelson and others, 2005). Such profiles are typical of organic carbon rich-sediments, and are, to first order, linked to sedimentation rate (compare Berner, 1978; Niewohner and others, 1998). As shown in figure 4A (see Appendix 3 for data), $[SO_4^{2-}]$ decreases from 27.1 ± 1.0 mM at 1 cm depth to 1.35 mM at ~230 cm depth. An additional measurement from deeper within the gravity core yields a larger concentration measurement, but this is within error of the gravimetrically determined data. Pore water sulfate decreases from the sediment-water-interface to the sulfate-depletion of depth at ~230 cm. Pore water methane reaches concentrations >1 mM at depths greater than 180 cm, giving a sulfate methane transition zone from approximately 175 to 225 cm. The concentration of dissolved inorganic carbon, DIC, increases from ~3 mM at 1 cm depth approximately linearly to ~40 mM at 150 cm depth, where the slope changes and the concentration gradient decreases. Berelson and others (2005) postulated that this change in slope is the combination of both the reaction stoichiometries of sulfate reduction and anaerobic methane oxidation, but also the presence of persistent pool of reactive organic carbon below the sulfate depletion depth.

The modeled organic carbon remineralization rate (GRR) and methane oxidation rate (CH_{4OR}) were then used directly to calculate the sulfate reduction rate (see fig. 3). As mentioned previously, an assumption in the baseline model is that organic carbon is remineralized either via organoclastic sulfate reduction or methanogenesis.

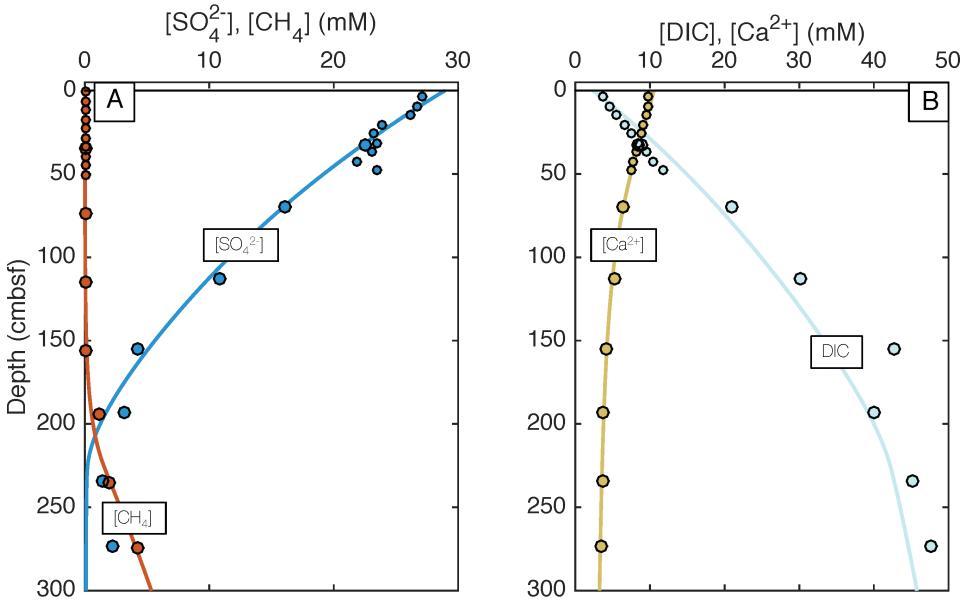

Fig. 4. (A) Model concentration outputs and Alfonso pore water data for $[SO_4^{2-}]$ and $[CH_4]$. The smaller data points (core top) are multi-core samples, and the larger data points are gravity core samples. The model fits are produced by parameterizing SRR as a function of organic carbon remineralization (GRR). See Appendix 1 for the details of the model construction. (B) Dissolved inorganic carbon (DIC) and pore water calcium (Ca^{2-}) concentrations and diagenetic model fits. The DIC profile is largely controlled by organic carbon remineralization, and Ca^{2+} is largely controlled by authigenic $CaCO_3$ precipitation.

Since anaerobic methane oxidation also has only sulfate as a terminal electron acceptor—by inference, all organic carbon that is remineralized in the model domain is ultimately oxidized with sulfate. The reaction stoichiometries of sulfate reduction, specified here as (C:S) of 0.6:1 and AOM of 1:1 determine the relationship between the rates of GRR, CH_4OR, and SRR (see fig. 3B). From the calculated rate profiles, however, it is possible to estimate the fraction of POC that is remineralized via sulfate reduction (~70%) versus that lost to AOM (~30%). These fractions agree with those estimated in Berelson and others (2005), and are within the range determined for typical organic carbon-rich margin sediments. The output SRR, of course, is the modulating factor for determining the sulfate concentration profile, and accurately reproduces the pore water data at depths <200 cm (fig. 4A). Analytical data from deeper in the core is itself noisier, and the values >2 mM are likely a sampling artifact. Thus, the column-integrated SRR yields remineralization rates matching sulfate flux estimates of 400 mmol $S/m^2\,y^{-1}$. As a check, Berelson and others (2005) computed the DIC flux across the sediment-water interface in Alfonso Basin as ~660 mmol $/m^2\,y^{-1}$, which, using the stoichiometry specified here equates to ~390 mmol $S/m^2\,y^{-1}$. This agreement serves to validate the model presented herein.

Isotopic Considerations

The measured $\delta^{34}S$ for pore water sulfate increases with depth (see fig. 5) as is typical of margin sediments, reflecting the preferential consumption of $^{32}SO_4^{2-}$ by microbial sulfate reduction in pore waters. We were materially limited for most of the samples deeper in the gravity core, but the pore water sulfate $\delta^{34}S$ values increase from seawater values $\delta^{34}S = 21.15 \pm 0.3$ permil (Johnston and others, 2014) to 33.0 permil

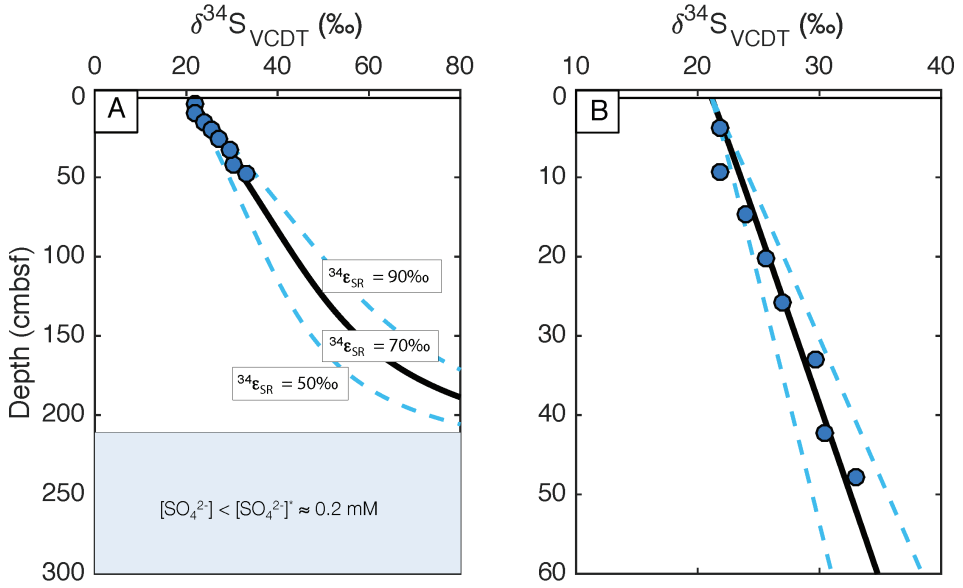

Fig. 5. (A) Pore water $\delta^{34}S_{SO4}$ values with respect to depth, and corresponding model fits output by the triple isotope reaction transport model. The model uses bulk SRR as an input and recalculates isotope specific rates using fractionation factors ($^{34}\alpha_{SR}$). The model fits here demonstrate that the best fit comes with a large applied fractionation associated with sulfate reduction ($^{34}\varepsilon_{SR}$ = 70‰). Here, the modeled sulfate reduction is all sulfate reduction, meaning that both organoclastic and methane oxidation carry the same fractionation. This should be further investigated in future studies. Other model fits demonstrate the range of possibilities in $\delta^{34}S$ gradients from different applied fractionation factors ($^{34}\varepsilon_{SR}$ = 50 and 90‰). (B) Same data and models as in (A), but for the depth range covered by the multicore data. The analytical precision on $\delta^{34}S$ values including chemistry and measurement is ±0.3‰.

at approximately 48 cm depth, where [SO_4^{2-}] has dropped to ~22 mM (fig. 5). Less intuitive is the increase in $\Delta^{33}S$ values with depth (see fig. 6), rising from near seawater values of 0.047 (±0.006‰) to 0.089 (±0.006‰) at 48 cm depth. A few other studies have observed similar behavior in pore waters (Johnston and others, 2008; Pellerin and others, 2015), and the closed-system consumption of sulfate (via MSR) would lead to similar behavior (increases in the values of both $\delta^{34}S$ and $\Delta^{33}S$ - Ono and others, 2006). For example, rayleigh distillation predicts a similar trajectory in $\delta^{34}S$ vs. $\Delta^{33}S$ when $^{34}\alpha_{SR}$ and $^{33}\lambda_{SR}$ values typical of laboratory culture MSR experiments are chosen. Clearly, the model used to explain the Alfonso Basin is more sophisticated, but the point is the same – mass balance can carry isotopic consequences similar to that seen in pore waters.

Perhaps most importantly, the primary goal of this study is to determine if the relationship between sulfate reduction rate and isotopic fractionation observed in experimental, lab-based pure culture studies is captured in marine sediments (Leavitt and others, 2013). The isotopic model inputs were tunable in the choice of down core behavior of $^{34}\varepsilon_{SR}$ and $^{33}\lambda_{SR}$, while still taking the SRR from the same bulk geochemical model. In essence, this allows a sensitivity test on the choice of input fractionation factors. Recognizing that closed-system modeling of sulfate reduction yields an increase of both $\delta^{34}S$ and $\Delta^{33}S$ values (Johnston and others, 2008; Pellerin and others, 2015), it is important to highlight that sedimentary systems are open to diffusive and advective exchange with overlying seawater. This results in a series of important conclusions. First, pore water $\delta^{34}S$ and $\Delta^{33}S$ values cannot be used directly to compute intrinsic environmental $^{34}\alpha_{SR}$ and $^{33}\lambda_{SR}$ values, as is often done and as would be

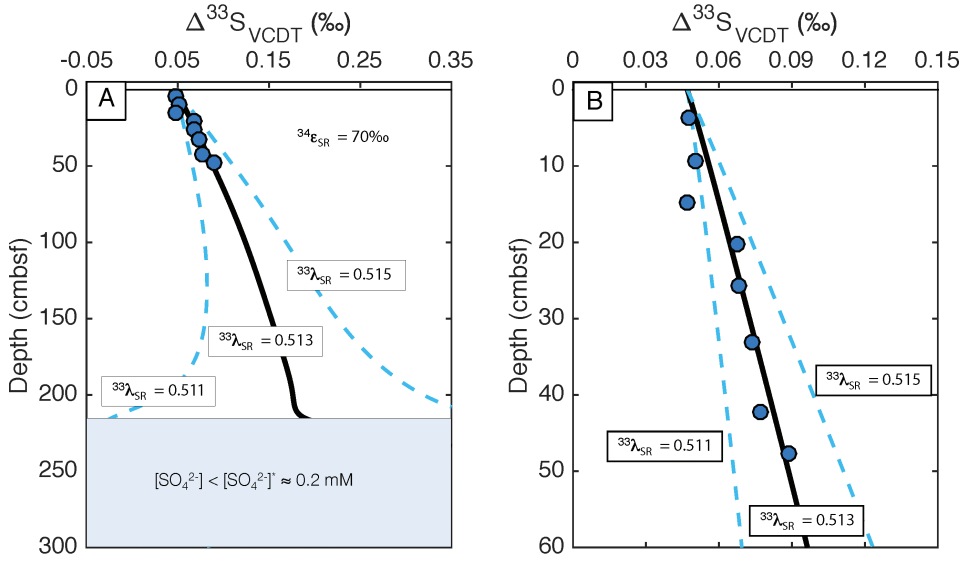

Fig. 6. (A) Pore water $\Delta^{33}S_{SO4}$ values with respect to depth, and corresponding model fits output by the triple isotope reaction transport model. The model uses bulk SRR as an input and recalculates isotope specific rates using fractionation factors ($^{34}\alpha_{SR}$), and the 'exponent' $^{33}\lambda_{SR}$, which relates that two fractionation factors ($^{33}\alpha_{SR}$ and $^{34}\alpha_{SR}$). The model outputs shown here were run with a constant $^{34}\varepsilon_{SR}$ = 70‰, but variable $^{33}\lambda_{SR}$ values. A value of $^{33}\lambda_{SR}$ ~0.513 fits the data, and the other fits demonstrate the model $\Delta^{33}S$ gradients with $^{33}\lambda_{SR}$ values = 0.511 and 0.515). (B) Same data and models as in (A), but for the depth range covered by the multicore data. The measurement precision on $\Delta^{33}S$ values is ±0.006‰.

required in a Rayleigh approach. The seminal study that highlighted the consequence of considering sediments as closed systems demonstrated that Rayleigh modeling of sedimentary systems leads to erroneous estimates of the fractionation factors of biogeochemical processes (Jorgensen, 1979). Though the latter is still frequently used to infer information about *in situ* biological isotope effects, we submit that only properly constructed open system reaction-transport models can accurately predict information about biologically mediated isotope effects. The second key assumption that is explored with our approach is the requirement in a classic closed-system model that the fractionation factors be constant throughout the sediment stack, as opposed to allowing for a depth-dependence to the isotopic fractionation factors (or put differently, a rate dependence to the fractionation). Our model allows this later assumption to be directly tested.

With this in mind, we used the sulfur isotope reaction-transport model to estimate the intrinsic fractionation factors required to reproduce the pore water $\delta^{34}S$ and $\Delta^{33}S$ profiles. We begin by simply holding the fractionation constant throughout the sediment column. As shown in figures 5 and 6, to reproduce the pore water $\delta^{34}S$ values requires a large fractionation associated with sulfate reduction ($^{34}\alpha_{SR}$ = 1.070, $^{34}\varepsilon_{SR}$ = 70‰, r^2 = 0.96). As a measure of the sensitivity of the model result to the choice of $^{34}\alpha_{SR}$, the figures also include results where $^{34}\varepsilon_{SR}$ = 50‰ (r^2 = 0.71) and 90‰ (r^2 = 0.78). Model fits using 60‰ < $^{34}\varepsilon_{SR}$ <80‰ all give r^2 > 0.90. Repeating a similar exercise in varying $^{33}\lambda_{SR}$, a similar approach can be undertaken to determine the best fit to the pore water $\Delta^{33}S$ data. In this case, $^{34}\alpha_{SR}$ is fixed at 1.070, and a $^{33}\lambda_{SR}$ value of 0.5130 (r^2 = 0.85, see fig. 6) best reproduces the pore water $\Delta^{33}S$ data. Other model $\Delta^{33}S$ outputs shown result from $^{33}\lambda_{SR}$ = 0.5110 (r^2 = 0.25) and $^{33}\lambda_{SR}$ = 0.5150 (r^2 = 0.25). The combination of these results is captured in a triple isotope plot (fig. 7), where

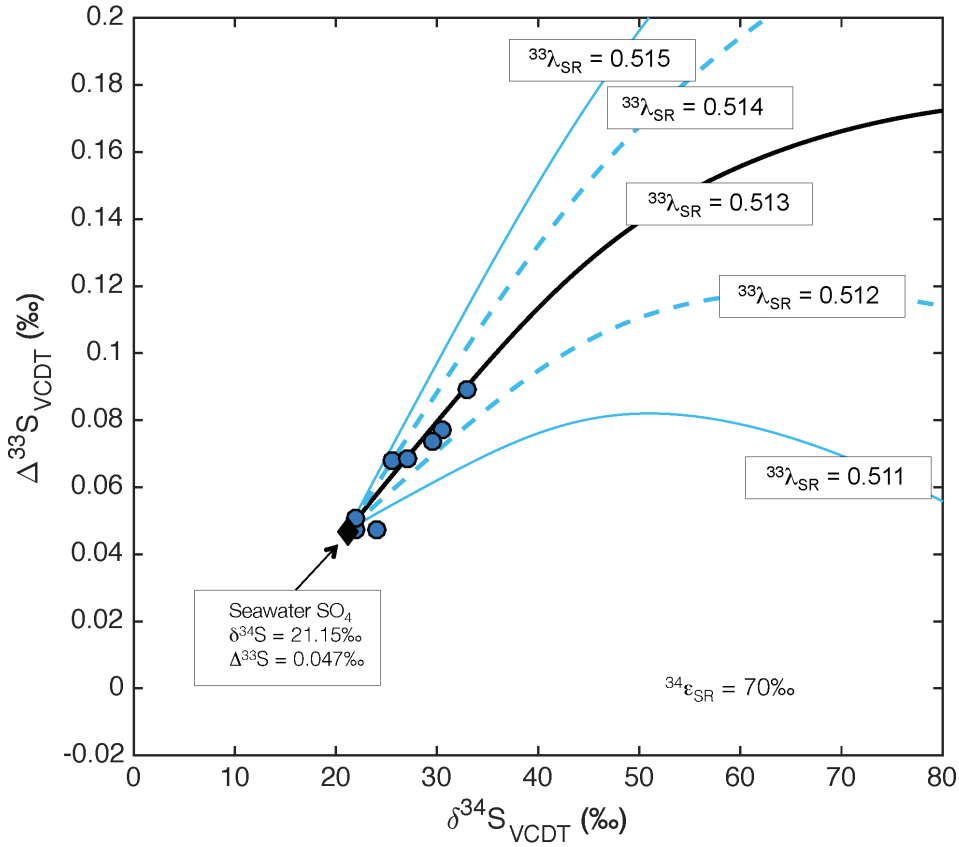

Fig. 7. Triple isotope plot ($\Delta^{33}S_{SO4}$ versus $\delta^{34}S_{SO4}$) of Alfonso pore water sulfate that plots the model outputs from figures 5 and 6 concurrently and shows the range provided by variable $^{33}\lambda_{SR}$ values. It is noteworthy that $^{33}\lambda_{SR} = 0.515$—on the reference frame defined by $\Delta^{33}S$ has a high positive trajectory—and is the isotopic consequence of partially closed system loss of pore water sulfate via microbial sulfate reduction. For reference, the isotopic composition of seawater sulfate is ($\delta^{34}S_{SO4} = 21.15 \pm 0.3‰$, $\Delta^{33}S_{SO4} = 0.0475‰$).

increasing depth is represented as the distance along the vector extending to the upper right and away from the composition of seawater sulfate (the boundary condition).

We can also consider the consequences of changing fractionation with depth. This could manifest as a linear dependence of fractionation on SRR, or an exponential dependence on SRR, like that seen in pure culture studies (Leavitt and others, 2013). Each of the scenarios results in a different $^{33}\alpha$ and $^{34}\alpha$ applied at variable depths within the model domain, and results in depth-dependent ^{32}SRR, ^{33}SRR, and ^{34}SRR (in all cases, isotope mass balance was conserved and checked such that SRR = ^{32}SRR + ^{33}SRR + ^{34}SRR).

Each of these different model solutions carries a different prescription between SRR and isotope fractionation. In the first test scenario, we explored a linear dependence of $^{34}\varepsilon_{SR}$ on rate (at SRR_{max}, $^{34}\varepsilon_{SR} \approx {}^{34}\varepsilon_{max}$ and vice versa). Here we used the same regressed values as determined in Leavitt and others (2013):

$$^{34}\varepsilon_{SR} = \frac{-39.3}{SRR_{max} - SRR_{min}} SRR + 56.5. \quad (5)$$

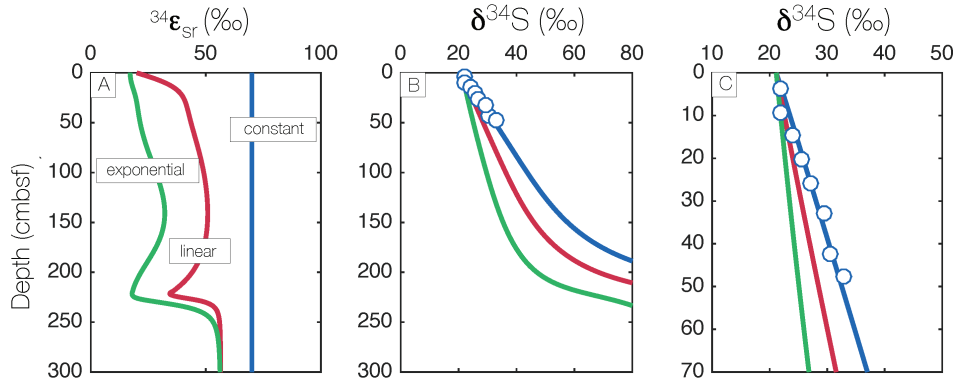

Fig. 8. Isotope model fits ($\delta^{34}S_{SO4}$ vs. depth) for different parameterization scenarios (constant $^{34}\varepsilon_{SR}$, linear dependence of $^{34}\varepsilon_{SR}$ on SRR, and exponential dependence of $^{34}\varepsilon_{SR}$ on SRR). The panels demonstrate (A) the input $^{34}\varepsilon_{SR}$ as a function of depth, as determined from the different parameterization scenario (B) the model $\delta^{34}S_{SO4}$ profile fit for each of the scenarios in (A), plotted with the multi-core $\delta^{34}S_{SO4}$ Alfonso Basin data throughout the entire model domain sampled by the gravity core (C), the $\delta^{34}S_{SO4}$ for the top 70 cm, the region sampled by the multicore.

In the next test case, we parameterized the exponential connection between SRR and $^{34}\varepsilon_{SR}$ using the model values from Leavitt and others (2013), where $^{34}\varepsilon_{min} = 17.2 \pm 1.3‰$ and $^{34}\varepsilon_{max} = 56.5 \pm 2.6‰$. Thus, the equation can be written as:

$$^{34}\varepsilon_{SR} = 39.3e^{-10(SRR - SRR_{min})} + 17.2 \quad (6)$$

with an attenuation coefficient of 10.

A comparison of the modeled fractionation factors (fig. 8), the whole core isotope model profile and the core topmodel profile demonstrates the isotopic behavior of each of the different scenarios. From this, we can highlight several key points. For both the linear and exponential cases, where the fractionation factor is a function of rate, a maximum fractionation factor of $^{34}\varepsilon_{max} = 56$ permil is insufficient to capture the behavior of the pore water sulfate $\delta^{34}S_{SO4}$ values. Although the $^{34}\varepsilon_{max}$ and $^{34}\varepsilon_{min}$ are the same in both cases, and values of $^{34}\varepsilon_{max}$ converge at depths where SRR decays to zero. The modeled isotope gradient in the exponential case is shallower than in the linear case because $^{34}\varepsilon_{SR}$ increases more slowly. Furthermore, the modeled $\delta^{34}S_{SO4}$ profiles largely do not reflect the structure of the $^{34}\varepsilon_{SR}$ input profile, a consequence of diffusive/advective transport of $^{32}SO_4^{2-}$, $^{33}SO_4^{2-}$ and $^{34}SO_4^{2-}$.

In all cases (exponential, linear, and constant), the sulfate $\delta^{34}S_{SO4}$ profile gradients are approximately linear with respect to depth down to 150 cm, where $[SO_4^{2-}] \approx 5$ mM. Utilizing different $^{34}\varepsilon_{min}$, fit to the highest SRR at shallow depths and ranging from $^{34}\varepsilon_{min} = (20‰–50‰)$, that same linear behavior in the sulfate isotope gradient is observed. Although a small change in the slope of $\delta^{34}S_{SO4}$ versus depth is observed, the chosen value of $^{34}\varepsilon_{max}$ has a much stronger influence on the sulfate isotope gradient than does $^{34}\varepsilon_{min}$. It is, of course, possible to model the $\delta^{34}S_{SO4}$ gradient with $^{34}\varepsilon_{max} > 70$ permil, in both the linear and the exponential case. The profile behavior is largely insensitive to the chosen $^{34}\varepsilon_{min}$ when $^{34}\varepsilon_{max}$ is large (>70%). Despite the fact that there is pronounced structure in $^{34}\varepsilon_{SR}$ associated with the sulfate depletion depth, there is comparatively little influence on the resultant $\delta^{34}S_{SO4}$ profile. In the case where $^{34}\varepsilon_{SR}$ is held constant, independent of SRR, and by inference depth, the best model fit to the isotope profile is produced when $^{34}\varepsilon_{SR} = 70$ permil (see fig. 8). The model $\delta^{34}S_{SO4}$ gradient is also linear with respect to depth until ~150 cm, when

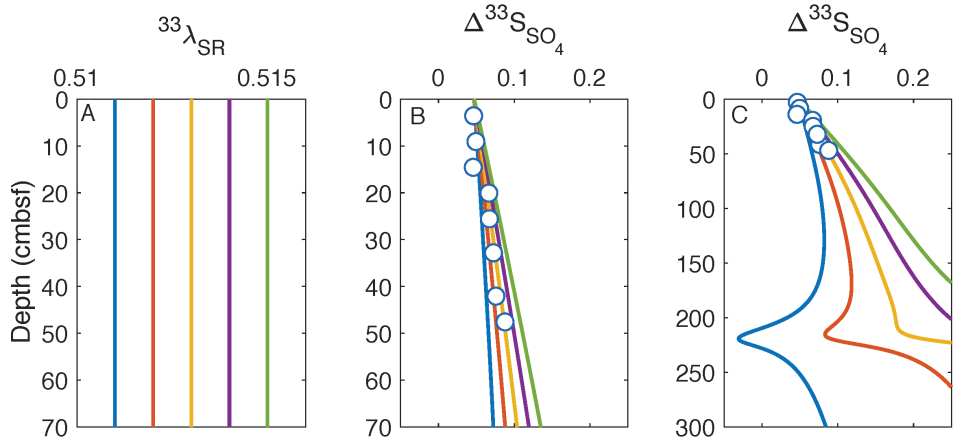

Fig. 9. Isotope model fits ($^{33}S_{SO4}$ vs. depth) for different parameterization scenarios. Like figure 8, (A) is a constant $^{33}\lambda_{SR}$, (B) is a linear dependence on $^{33}\lambda_{SR}$, and (C) is the exponential dependence on $^{33}\lambda_{SR}$. In each case, $^{34}\varepsilon_{SR}$ is 70 ‰.

the sulfate concentration profile also begins to approach the sulfate depletion depth. All $^{34}\varepsilon_{SR}$ input values into the model where $^{34}\varepsilon_{SR} < 60$ permil produce a $\delta^{34}S_{SO4}$ gradient that is too shallow, all input $^{34}\varepsilon_{SR} > 80$ permil produce a $\delta^{34}S_{SO4}$ gradient that is too large to accurately reproduce the measured pore water sulfate samples within Alfonso Basin. Although the constant $^{34}\varepsilon_{SR}$ scenario was tested simply as an end member case, we acknowledge that it provides the best fit with the least number of assumptions (the most conservative approach) to the $\delta^{34}S_{SO4}$ values and accurately reproduces the pore water $\delta^{34}S_{SO4}$ gradient in the top 50 cm. Therefore, a scenario that parameterized the connection between $^{34}\varepsilon_{SR}$ and SRR is not necessary. Further, it is critical to acknowledge that the physical transport of sulfate (diffusive and advective) results in the loss of information about the fractionation behavior at the reaction level.

In a similar fashion to that outlined above, it is possible to demonstrate a series of model fits to the pore water sulfate $\Delta^{33}S_{SO4}$ values. Noting that the variability in $\Delta^{33}S_{SO4}$ values are modest over the measured range (increasing from near seawater sulfate values at the seawater interface of 0.047 ± 0.006‰ to 0.086 ± 0.006‰ at 47 cm depth). Importantly, only minute variability in $^{33}\lambda_{SR}$ is required to produce substantial changes in the trajectory of $\Delta^{33}S_{SO4}$ versus depth. Demonstrating a sensitivity test, figure 9 exhibits the influence of variable, rate-independent $^{33}\lambda_{SR}$ on the output pore water sulfate $\Delta^{33}S_{SO4}$. While not all of these values are physically reasonable given the $^{34}\varepsilon_{SR}$, several features are notable. First, increasing $^{33}\lambda_{SR}$ with constant $^{34}\varepsilon_{SR}$ produces a more rapid increase in the $\Delta^{33}S_{SO4}$ model output. This is an expected result, as $^{33}\lambda_{SR}$ relates the fractionation factors $^{33}\alpha_{SR}$ and $^{34}\alpha_{SR}$, larger values of $^{33}\lambda_{SR}$ produce a relatively larger enrichment in ^{33}S. Secondly, despite the fact that $\Delta^{33}S$ is calculated within the reference frame $^{33}\lambda = 0.515$, values of $^{33}\lambda_{SR} > 0.510$ are sufficient to produce a positive trajectory in triple isotope space ($\delta^{34}S_{SO4} - \Delta^{33}S_{SO4}$). It is possible that some closed system behavior, such as can be observed in pore waters, partially explain this trajectory. Thirdly, with the application of both constant $^{34}\varepsilon_{SR}$ and $^{33}\lambda_{SR}$, non-linear trajectories are observed in the triple isotope composition of pore water sulfate. Whereas simple, Rayleigh-like models of sulfate in closed systems demonstrate linear arrays (Ono and others, 2006), the model trajectories for a diagenetic model like that constructed here are more complex as sulfate is consumed.

The combination of $^{34}\alpha_{SR}$ and $^{33}\lambda_{SR}$ is mechanistically meaningful. A central goal of this study is to test and explore the implications of these paired fractionation factors in light of both thermodynamic constraints and laboratory/experimental studies. The primary result of this test, and perhaps this entire study is that the fit to the isotope data and preferred model solution does not require that the fractionation factors be changing with depth or SRR. This could also reflect the overall low metabolic rates (relative to the lab) in natural systems. Thus, using a fixed fractionation value is the most conservative approach.

The Uniqueness of Alfonso Basin Sediments

The analysis given above provides quantitative evidence for the contributions of microbial sulfate reduction and physical transport to an observed pore water sulfate profile. Much of this analysis, however, is tightly linked to the specific geochemical and sedimentological environment present in Alfonso Basin. The question then becomes: is the observation at Alfonso Basin similar to what can be found more broadly in other early diagenetic environments? Sulfate concentration profiles from a wide range of different environments are present in the literature, and Alfonso Basin is unexceptional in this sense. Further, there are numerous cases where the $\delta^{34}S_{SO4}$ of pore water sulfate has been included. Much like that for sulfate concentrations, there is broad similarity between the down core behavior of $\delta^{34}S_{SO4}$ values and $[SO_4^{2-}]$. This has commonly been the motivation for using a closed-system, Rayleigh model to describe this isotopic behavior. However, as we note from above, transport is also a key feature in discerning a strictly microbial feature within marine pore water profiles – a distinction that was aided by the inclusion of $\Delta^{33}S_{SO4}$ measurements. Thus, to begin to address the broader applicability of ^{33}S and the model presented above, we present pore water sulfate data ($\delta^{34}S_{SO4}$ and $\Delta^{33}S_{SO4}$) from three other California-Mexican margin sites: Mazatlan, Santa Monica Basin, and San Blas.

A full, Alfonso Basin-like model treatment of these other data sets is outside the scope of this study, given that the requisite supporting data are largely unavailable. However, the uniqueness of the minor sulfur isotope signature identified in Alfonso Basin sediment pore water can serve as a proxy for whether the Alfonso result is more broadly applicable. In figure 10, we present data from the other margin basins. What is immediately clear is that there is a general consistency between the Alfonso Basin profiles and the other margin sites. That noted, there are also potential differences. It is first important to note that pore water sulfate measurements from the other basins cover a wide range of sulfate concentrations, always beginning with bottom waters as the boundary condition, and carrying seawater sulfate values. Like the Alfonso Basin, as sulfate is reduced in other basinal sediments, the $\delta^{34}S_{SO4}$, and $\Delta^{33}S_{SO4}$ values increase. The overwhelming trend across all basins is a reasonably defined trajectory in $\delta^{34}S_{SO4} - \Delta^{33}S_{SO4}$ values (positive slope in quadrant 1). That noted, there is variability outside of analytical precision between the localities. The root of this variance is a target for further research as it could be related to any one of the various parameters that come to control the early diagenesis of sulfur. Fortunately, the general consistency among the observations leaves the inclusion of ^{33}S as a promising direction for further study.

Implications and Extrapolation

There are several environmental and sedimentary implications stemming from the interpretation of the diagenetic model built to explain the Alfonso Basin sulfate pore water sulfate isotope profile. The model results for this site define an intrinsic, or net fractionation for sulfate reduction of $^{34}\varepsilon_{SR} = 70$ permil, with an accompanying $^{33}\lambda_{SR}$ of 0.5130. Until recently, researchers postulated that the natural upper limit of sulfur isotope fractionation via MSR was $^{34}\varepsilon_{SR} \sim 46$ permil (Peck, 1959; Peck, 1961; Kemp and Thode, 1968; Rees, 1973; Habicht and Canfield, 1997; Johnston, 2011). As it

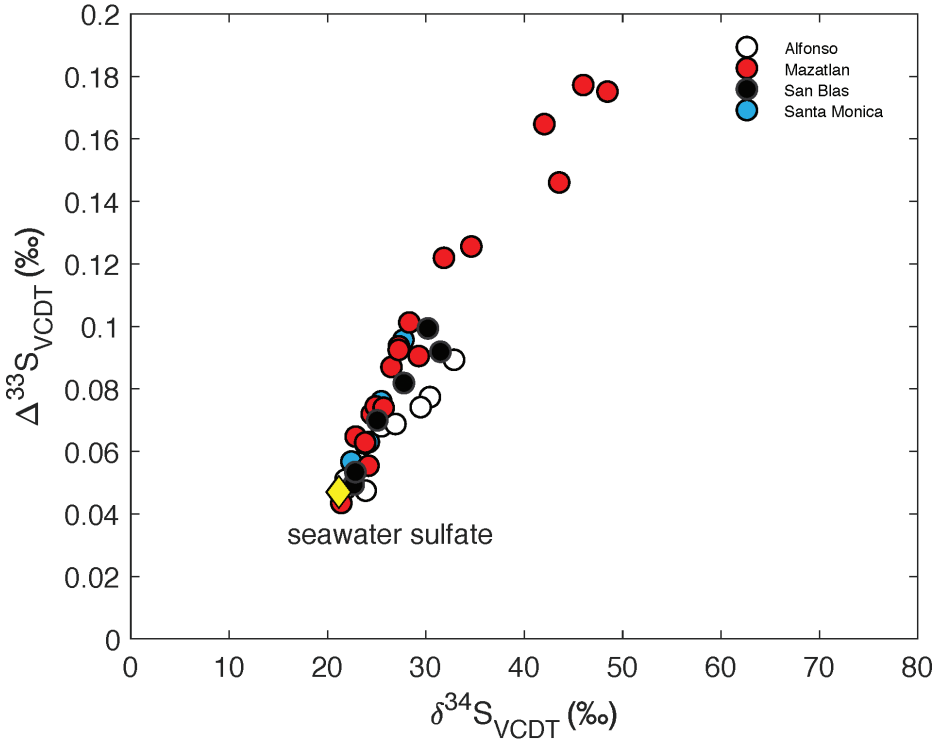

Fig. 10. Triple isotope plot ($\Delta^{33}S_{SO4}-\delta^{34}S_{SO4}$) of pore water sulfate sampled during the CalMex (2001) cruise, with Alfonso, Mazatlan, Santa Monica, and San Blas Basins. All four basins are anoxic silled basins of the California-Mexican margin. The pore water sulfate displayed here is largely from the multicores sampled during that cruise, except for Mazatlan, which also includes gravity core sulfate. Seawater sulfate is included for reference ($\delta^{34}S_{SO4} = 21.15 \pm 0.15‰$ and $\Delta^{33}S_{SO4} = 0.047 \pm 0.006‰$).

is common for the isotopic offset between pore water sulfate and free sulfide (or pyrite) to exceed this presumed limit, oxidative sulfur cycling was frequently invoked to explain environmental measurements exceeding this value (Habicht and Canfield, 1997; Habicht and others, 1998). Not only did this carry consequences for studying S cycling in modern systems, it also carried implications for interpreting S cycling through geological proxy records (for example, $BaSO_4$, $CaSO_4$, and sedimentary pyrite) (Canfield and Teske, 1996; Strauss, 1999; Canfield, 2001; Canfield, 2004; Canfield and Farquhar, 2009). Despite the lack of laboratory evidence that sulfur isotope fractionations could exceed ~46 permil, theoretical metabolic models suggested that such was possible (Brunner and Bernasconi, 2005; Johnston and others, 2007; Johnston, 2011). These models used low-temperature thermodynamics as a guide, where calculations suggest sulfur isotope equilibrium between sulfate and sulfide approaches 70 to 80 permil at Earth surface temperatures. More recent experimental work has since demonstrated that microbial fractionations can exceed the canonical 46 permil value, both in laboratory experiments with single cultures of sulfate reducers (Sim and others, 2011; Leavitt and others, 2013) and in environmental systems such as stratified lakes (Canfield and others, 2010; Gomes and Hurtgen, 2013). First, this clearly changes the once necessary role of oxidative sulfur cycling. Further, an emerging picture highlights the importance of rates of sulfate reduction as playing a key role in setting the $^{34}\varepsilon_{SR}$ (Sim and others, 2011; Leavitt and others, 2013). More

specifically, biomass-normalized rates of sulfate reduction are inversely correlated with the magnitude of an expressed isotope effect. Low metabolic rates produce fractionations that approach 70 permil, and are a predictable consequence from equilibrium calculations and theoretical isotope modeling studies (compare Wing and Halevy, 2014). Higher metabolic rates approach a much smaller net fractionation. Thus, most laboratory studies are now converging on the ideas that metabolic rate is the governing physiological parameter that controls the magnitude of S isotope fractionation in sulfate reducers, with the added reality that MSR can carry large $^{34}\varepsilon$ effects. If this indeed holds, then the majority of environmental isotopic compositions can be accommodated by the isotope effects of sulfate reduction alone. Moreover, if the modeled fractionation factor demonstrated in this study (=70‰) is shared across environments more broadly, it would suggest that marine sediments – like those in Alfonso Basin – foster the type of environmental conditions that keep metabolic rates of *in situ* sulfate reduction operating near their lower physiological limit, and far below most laboratory studies.

It is important to revisit that the calculated SRR changes as a function of depth. Considering only the top 250 cm of the sediment column where sulfate reduction is actively taking place, the maximum bulk sulfate reduction rate is at the core-top, where $SRR_{max} = 1.7 \times 10^{-6}$ mol/(L·d). As expected, the minimum SRR is at the base of the sulfate reduction zone, and equals 0.027×10^{-6} mol/(L·d). Finally, in the range of sediment horizons where we have made sulfur isotope measurements (0–50 cm), SRR changes by a factor of 3. This offers an opportunity to further revisit the environmental manifestation of the rate – fractionation relationship derived from recent laboratory studies (Leavitt and others, 2013). Importantly, this is the first critical environmental test of this hypothesis. Recall that $^{34}\varepsilon_{SR}$ and $^{33}\lambda_{SR}$ are both coupled and correlated, scaling as a function of metabolic rate (see Leavitt and others, 2013). Recall also that the natural range of $^{34}\varepsilon_{SR}$ spans ~70 permil, whereas the natural mass-dependent range in $^{33}\lambda_{SR}$ is 0.5080 to 0.5150 (Johnston and others, 2008; Leavitt and others, 2013). As $^{34}\varepsilon_{SR}$ increases towards the maximum thermodynamically predicted value (roughly 70‰), $^{33}\lambda_{SR}$ also increases concomitantly, to a value of approximately 0.5150 (the basis for the $\Delta^{33}S$ reference frame: Farquhar and others, 2003). In diagenetic model treatment of Alfonso Basin, the two model input parameters – $^{34}\varepsilon_{SR}$ and $^{33}\lambda_{SR}$ - are treated as functionally independent with a best fit of $^{34}\varepsilon_{SR} = 70$ permil and $^{33}\lambda_{SR} = 0.5130$. This set of best fit fractionation factors can then be directly compared to the $^{34}\varepsilon_{SR} - ^{33}\lambda_{SR}$ pairs from published MSR experiments. Interestingly, this exercise yields only a loose consistency between our model prediction and pure culture studies.

The expectation from thermodynamic predictions, and as realized in microbial experiments (Leavitt and others, 2013; Wing and Halevy, 2014), is that when $^{34}\varepsilon_{SR}$ approaches an equilibrium value, the $^{33}\lambda_{SR}$ should follow suit and carry a value near 0.5145 to 0.5150. The product 0.5130 from our treatment, with a concomitant $^{34}\varepsilon_{SR}$ of ~ 70 permil, is thus unexpected and out of step with pure equilibrium calculations. This offset may be due to a number of factors. First, it is always possible that there is a fundamental difference in the behavior of MSR in marine sediments relative to our common laboratory strains. This could be purely physiological or speak to the behavior of a mixed community of organisms (in sediments) as opposed to the pure cultures in the laboratory. It is also possible that the environmental conditions – and thus physiological state – of the laboratory culture insufficiently mimics that of marine sediments. Finally, it is possible that the slight mismatch between model fits and equilibrium predictions could reflect contributions from other metabolic processes active in marine sediments. This would not augment equilibrium predictions proper, but would allow for additional (and largely unknown) kinetic effects. In all of these cases, laboratory cultures are a good first-step toward interpreting sedimentary data, but necessarily incomplete. Fortunately, these types of features are testable.

It is also important to acknowledge a limitation of the current data set. That is, given the mass requirements for isotope analyses, only the upper reaches of the core were accessible for analysis. Having access to pore water sulfate samples from the full length of the pore water sulfate column would certainly improve our understanding of the deep-core behavior of MSR. There is also the opportunity to extend this style of analysis to a more appropriate relation to experimental data, drawing in (for instance) data on biomass loads and cell counts. Recall that the model generates bulk geochemical rates, which differ from the normalized rates extracted from experimental microbiology.

Direct cell counts are absent from Alfonso Basin sediments, however estimates exist for other typical margin sediments. From this work, cell numbers range from 10^6 to 10^{10} cells/cm^3 for the top 10 cm, decreasing with depth (Parkes and others, 2014). We can use these general down core observations to provide an order-of-magnitude estimate of the cell-specific reduction rates in Alfonso Basin sediments. These estimates are based upon on our modeled rate profile, with $SRR_{max} = 1.7 \times 10^{>9}$ mol/cm^{3}d and $SRR_{min} = 2.7 \times 10^{>11}$ mol/cm^{3}d. These are then simply converted to cell-specific rates, following:

$$csSRR_{max} = \frac{SRR_{max}}{cell\#} \tag{7}$$

$$csSRR_{min} = \frac{SRR_{min}}{cell\#}. \tag{8}$$

Over the range sulfate reduction rates measured for Alfonso Basin, we calculate that csSRR = $1.7 \times 10^{-15} - 1.7 \times 10^{-19}$ mol/cell*d is the upper limit for 10^{10} cells/cm^3, and 2.7×10^{-17} and 2.7×10^{-21} for 10^6 cells/cm^3. A noteworthy consequence of this calculation is that, despite the ~100x range in modeled bulk rates for this particular sediment column, the computed range of cell-specific sulfate reduction rates for Alfonso Basin sediments are significantly below those generated in the laboratory calibration of Leavitt and others (2013). Since the lowest rates in Leavitt and others ($\sim 10^{-12}$ mol/cell*d) were characterized by sulfur isotope fractionations >50 permil, it is reasonable to suggest that the natural sulfate reduction rates of microbial communities in Alfonso Basin are slow enough to explain the large sulfur isotope fractionation in the modeled profile. In both experiments and the pore water condition, rates are modulated by the reactivity and/or delivery of organic carbon. Further, this does not explain the mismatch in $^{33}\lambda_{SR}$, but does allow for a significant step toward bridging between experimental and environmental data. It further points to the common behavior MSR in marine sediments operating at exceedingly low metabolic rates. If, as proposed, low net metabolic rates suggest a high degree of dissimilatory pathway reversibility (Wing and Halevy, 2014), then these low rates would also carry the isotope effect associated with chemical equilibrium.

CONCLUDING REMARKS

Laboratory based studies recently highlighted the dependence of metabolic rate of sulfate reduction on the magnitude of the product sulfur isotopic effect. It is then tempting to revisit geological records of sulfur isotope fractionations and interpret these changes based solely as a function of metabolic rate. In this study, we examine whether isotope fractionation, as preserved in marine pore water sulfate, carries a memory effect of changes in microbial metabolic rates. In order to address this question, we analyzed a geochemically well-characterized core for the triple isotopic composition of pore water sulfate. We also formulated a reaction-transport diagenetic model for a sedimentary system in order to quantitatively understand the triple S isotope characteristics and its relationships to microbial calibrations of sulfur metabolisms.

The model reproduces the profiles of the major pore water species, including [SO_4^{2-}], [CH_4], DIC, and Ca^{2+}, and generates realistic sulfate reduction and methane oxidation rate profiles that corroborate previously published data. The sulfate reduction rate profile is then used, in concert with isotopic fractionation parameters, to evaluate the intrinsic isotopic characteristics of sedimentary sulfate reduction required to reproduce the triple isotope behavior of pore water sulfate within Alfonso Basin. From this we find a best-fit solution is where $^{34}\varepsilon_{SR}$ and $^{34}\lambda_{SR}$ are invariant with depth/rate with values of 70 permil and 0.5130, respectively. No change in the intrinsic fractionation is necessary to account for the down core, evolving multiple isotope composition of sulfate. That noted, this result is constrained by the observational window presented herein, where we cover ~50 cm of depth, a 3X change in SRR and 20 percent of pore water sulfate removal. It is possible that in cases where a larger SRR range is sampled, and/or a larger range in $\delta^{34}S$, such a relationship remains. The model framework presented here is directly transferable to such a study.

We demonstrate that pore water isotope signatures are consistent with very low *in situ* specific rates of sulfate reduction – despite the fact that Alfonso Basin is an organic carbon-rich marginal setting. However, the triple isotope signatures ($\delta^{34}S/\Delta^{33}S$) are still within the range of the predictions from laboratory calibrations of sulfate reducers, and no additional need for S cycling (oxidation/disproportionation) is required to produce the pore water $\Delta^{33}S_{SO4}$ profile. Despite the challenges in assessing a potential rate relationship to fractionation, our work further reinforces that physical transport (advection and diffusion) significantly contributes to observed isotopic behavior of pore water sulfate. The isotopic composition of pore water sulfate thus records more than biogeochemical processes and must be interpreted in the light of this finding. Future studies would benefit from whole core samples and more in-depth consideration of the triple isotope composition of other pore water and solid phase S species.

ACKNOWLEDGMENTS

We thank Erin Beirne for laboratory assistance, Itay Halevy for thoughtful discussions, and the crew of New-Horizons for assistance with coring and sampling during the cruise of 2001. A.L.M. is funded through Harvard University Peirce Fellowship. This work is supported by an NSF instrument grant and NASA Astrobiology Institute to D.T.J. Financial support for this work was provided to WB via NSF grant OCE 0727123. The authors would like to acknowledge the coring, pore water extraction and analytical help of O. Gonzalez-Yajimovich, J. McManus, M. Prokopenko, L. Chong and N. Rollins. The authors would like to thank D. Canfield, D. Burdige and T. Komada for thoughtful comments on the manuscript.

APPENDIX 1

Derivation of the Terms GRR and SRR in the Bulk Geochemical Reaction Transport Model (RTM)

Diagenetic reaction transport models have been extensively applied over the past 50 years (compare Berner, 1964), and have been the subject of numerous papers. The mathematics behind them have also been fleshed out in two textbooks that are still the standard references on the subject (Berner, 1980; Boudreau, 1997). We apply a few of the formulations here to derive the equations used in the bulk geochemical model, and to demonstrate how rates are calculated from the concentrations of pore water species.

Using a combination of finite difference methods, the steady-state reaction transport equation for a solute c in a porous medium is defined as (from Berner, 1980):

$$\frac{d}{dx}\left(\varphi D_s \frac{dc_{pw}}{dx}\right) - \frac{d}{dx}(\varphi \nu c_{pw}) + \varphi \sum R_{pw} = 0, \tag{A1.1}$$

where,

$$\varphi\nu = \varphi_\infty \omega_\infty, \tag{A1.2}$$

and

$$D_s = \frac{D}{\theta^2} \tag{A1.3}$$

We employ a well-known relationship that defines tortuosity – the mean path of a solute through a porous medium (Ullman and Aller, 1982) as,

$$\theta^2 = \varphi^{m-1}. \tag{A1.4}$$

Above φ is the depth-dependent porosity, D_S is the bulk sediment diffusion coefficient, c_{pw} is the concentration of the species in pore water, φ_∞ and ω_∞ are the porosity and sedimentation rate at infinite depth—the lower depth boundary. The term ΣR_{PW} is sum of all the reaction terms influencing the pore water concentration of c.

For solid phase components, the terms are simplified due to a lack of diffusion and bioturbation (where ρ_{sm} is constant), and the steady state equation becomes:

$$-\frac{d}{dx}[(1-\varphi)\omega c_{ds}] + (1-\varphi)\sum R_{ds} = 0 \tag{A1.5}$$

and

$$(1-\varphi)\omega = (1-\varphi_\infty)\omega_\infty. \tag{A1.6}$$

In this case, c_{ds} is the concentration of the species in the dry sediment. To parameterize OC remineralization, we employ a '3G' model, consisting of three 'reactive' POC fractions that are binned by reactivity, and carry unique remineralization constants (k_1, k_2, k_3). As model inputs, f_1 and f_2 are the fractions of G_1, and G_2 in the total reactive pool G, and thus the concentrations of G_1, G_2, and G_3 are determined as follows:

$$G_1 = f_1 \cdot G \tag{A1.7a}$$

$$G_2 = f_2 \cdot G \tag{A1.7b}$$

$$G_3 = (1 - f_1 - f_2) \cdot G \tag{A1.7c}$$

The fractions of G_1, G_2, and G_3 are computed in this way, are used to set the upper boundary conditions for the model. The determination for the organic carbon remineralization rate—termed GRR, with respect to pore water, is derived from the Runge-Kutta finite difference method for each of the reactive fractions (n = 1, 2, 3):

$$\frac{dG_n}{dx} = -k_n \frac{G_n(1-\varphi)}{\omega_\infty(1-\varphi_\infty)} \tag{A1.8}$$

$$GRR_{pw} = (k_1 G_1 + k_2 G_2 + k_3 G_3)\left(\frac{\rho_{sm}(1-\varphi)}{0.0012 \cdot \varphi}\right) \tag{A1.9}$$

The term GRR_{pw} has units of $\mu mol/cm^3/d$, whereas all of the fractions G are as wt% organic carbon. In the bulk model, GRR_{pw} is computed first, and is used to determine the sulfate reduction (SRR) and methane production (CH_4PR) rates. Implicit in this calculation is that all organic carbon remineralization taking place at depths where sulfate concentrations exceed a prescribed threshold ($[SO_4^{2-}] > [SO_4^{2-}]^*$) is via sulfate reduction (that is, no aerobic remineralization, no ferric iron reduction, *et cetera*). At any depth where $[SO_4^{2-}] < [SO_4^{2-}]^*$, remineralization takes place via methanogenesis. SRR also takes into account SO_4^{2-} consumed via methane oxidation (AOM). The calculation of SRR and GRR are demonstrated below:

$$SRR_{pw} = \gamma_1\left[\left(\frac{4-XS}{8}\right) \cdot GRR_{pw} + k_{MO}[CH_4]\right] \tag{A1.10a}$$

where:

$$\gamma_1 = 0.5\left[1 + erfc\left[\frac{[SO_4^{2-}] - [SO_4^{2-}]^*}{0.05}\right]\right] \tag{A1.10b}$$

Is the function that modulates SRR in the presence of sulfate limitation, to parameterize Monod kinetics. The term XS is the oxidation state of organic matter (Alperin and others, 1994). The rate of methanogenesis CH_4PR is thus:

$$CH_4PR = \gamma_2 \cdot \left[\left(\frac{4 - XS}{8} \right) \cdot GRR_{pw} \right] \tag{A1.11a}$$

where:

$$\gamma_2 = 0.5 \left[1 - erfc \left[\frac{[SO_4^{2-}] - [SO_4^{2-}]^*}{0.05} \right] \right] \tag{A1.11b}$$

This function γ_2 has a similar purpose as γ_1, but modulates the rates of methanogenesis due to sulfate inhibition about the prescribed sulfate threshold $[SO_4^{2-}]^*$. These two rates (SRR and CH_4PR) are employed in the finite difference diagenetic model that solves for the concentrations of $[SO_4^{2-}]$ and $[CH_4]$ by adjusting the parameters f_1, f_2, k_1, k_2, k_3 and k_{MO}.

APPENDIX 2

Derivation of Isotope (^{32}S, ^{33}S, and ^{34}S) Specific Rate Terms ^{32}SRR, ^{33}SRR, and ^{34}SRR, and Construction of the Steady-State Diagenetic Equations

The determination of isotope specific rates for the sulfur system has been detailed before for the two-isotope system (^{32}S and ^{34}S) (Jorgensen, 1979; Dale and others, 2009), and by similarity, it can be shown for the three-isotope system (^{32}S, ^{33}S, and ^{34}S). The algebraic solution shares some similarities with those for the two-isotope system, but naturally depends on two fractionation factors $^{33}\alpha_{SR}$ and $^{34}\alpha_{SR}$, which we have described in this paper as being mathematically linked via $^{33}\lambda_{SR}$ (eq. A2.12):

$$^{33}\lambda_{SR} = \frac{ln(^{33}\alpha_{SR})}{ln(^{34}\alpha_{SR})} \tag{A2.1}$$

The isotope-specific rates ^{32}SRR, ^{33}SRR, and ^{34}SRR depend on the concentrations of $[^{32}SO_4^{2-}]$, $[^{33}SO_4^{2-}]$, and $[^{34}SO_4^{2-}]$, but also on the rate constants $^{32}k_{SR}$, $^{33}k_{SR}$, and $^{34}k_{SR}$:

$$^{32}SRR = {}^{32}k_{SR} \cdot [^{32}SO_4^{2-}] \tag{A2.2a}$$

$$^{33}SRR = {}^{33}k_{SR} \cdot [^{33}SO_4^{2-}] \tag{A2.2b}$$

$$^{34}SRR = {}^{34}k_{SR} \cdot [^{34}SO_4^{2-}] \tag{A2.2c}$$

Intrinsic within the rate constants are the fractionations associated with sulfate reductions, and the fractionation factors are simply the ratios of those rate constants. This allows for the expression of the isotope-specific rate constants as functions of each other, linked via the fractionation factors:

$$^{33}\alpha_{SR} = \frac{\frac{^{32}SRR}{[^{32}SO_4^{2-}]}}{\frac{^{33}SRR}{[^{33}SO_4^{2-}]}} \quad \Rightarrow \quad {}^{32}SRR = {}^{33}SRR \frac{^{33}\alpha_{SR}[^{32}SO_4^{2-}]}{[^{33}SO_4^{2-}]} \tag{A2.3a}$$

$$^{34}\alpha_{SR} = \frac{\frac{^{32}SRR}{[^{32}SO_4^{2-}]}}{\frac{^{34}SRR}{[^{34}SO_4^{2-}]}} \quad \Rightarrow \quad {}^{32}SRR = {}^{34}SRR \frac{^{34}\alpha_{SR}[^{32}SO_4^{2-}]}{[^{34}SO_4^{2-}]} \tag{A2.3b}$$

Recalling that the bulk sulfate reduction rate is simply the sum of the isotope-specific rates (A2.4), the equations for the isotope-specific rates can be solved as functions of the bulk rate, the isotopologue concentrations, and the fractionation factors (A2.5a-c):

$$SRR = {}^{32}SRR + {}^{33}SRR + {}^{34}SRR \tag{A2.4}$$

$$^{32}SRR = SRR \left[\frac{^{33}\alpha_{SR}{}^{34}\alpha_{SR}[^{32}SO_4^{2-}]}{^{33}\alpha_{SR}{}^{34}\alpha_{SR}[^{32}SO_4^{2-}] + {}^{34}\alpha_{SR}[^{33}SO_4^{2-}] + {}^{33}\alpha_{SR}[^{34}SO_4^{2-}]} \right] \tag{A2.5a}$$

$$^{33}SRR = SRR \left[\frac{^{34}\alpha_{SR}[^{33}SO_4^{2-}]}{^{33}\alpha_{SR}{}^{34}\alpha_{SR}[^{32}SO_4^{2-}] + {}^{34}\alpha_{SR}[^{33}SO_4^{2-}] + {}^{33}\alpha_{SR}[^{34}SO_4^{2-}]} \right] \tag{A2.5b}$$

$$^{34}SRR = SRR \left[\frac{^{33}\alpha_{SR}[^{34}SO_4^{2-}]}{^{33}\alpha_{SR}{}^{34}\alpha_{SR}[^{32}SO_4^{2-}] + {}^{34}\alpha_{SR}[^{33}SO_4^{2-}] + {}^{33}\alpha_{SR}[^{34}SO_4^{2-}]} \right] \tag{A2.5c}$$

It is these rate determinations that appear in the final steady-state diagenetic equations for the isotope reaction transport model and derived from A2.3-4. By analogy to those described for the bulk geochemical model, they can be written as in equations A2.6a-c:

$$\varphi^2 D_0^{SO_4}\frac{d^2[^{32}SO_4^{2-}]}{dx^2}+\left(3\varphi D_0^{SO_4}\frac{d\varphi}{dx}-\frac{\omega_\infty\varphi_\infty}{\varphi}\right)\frac{d[^{32}SO_4^{2-}]}{dx}-{}^{32}SRR=0 \tag{A2.6a}$$

$$\varphi^2 D_0^{SO_4}\frac{d^2[^{33}SO_4^{2-}]}{dx^2}+\left(3\varphi D_0^{SO_4}\frac{d\varphi}{dx}-\frac{\omega_\infty\varphi_\infty}{\varphi}\right)\frac{d[^{33}SO_4^{2-}]}{dx}-{}^{33}SRR=0 \tag{A2.6b}$$

$$\varphi^2 D_0^{SO_4}\frac{d^2[^{34}SO_4^{2-}]}{dx^2}+\left(3\varphi D_0^{SO_4}\frac{d\varphi}{dx}-\frac{\omega_\infty\varphi_\infty}{\varphi}\right)\frac{d[^{34}SO_4^{2-}]}{dx}-{}^{34}SRR=0 \tag{A2.6c}$$

These equations are then solved using the exact same method as for the bulk geochemical model.

Derivation of Upper Boundary Conditions for [$^{32}SO_4$], [$^{33}SO_4$], and [$^{34}SO_4$] from $\delta^{34}S_{SO4}$, and $\Delta^{33}S_{SO4}$

For the case where [$^{36}SO_4^{2-}$] is excluded from consideration, [SO_4^{2-}] is the sum of the constituent species [$^{32}SO_4^{2-}$], [$^{33}SO_4^{2-}$], and [$^{34}SO_4^{2-}$], as below in eq. (A1.1)

$$[SO_4^{2-}]=[^{32}SO_4^{2-}]+[^{33}SO_4^{2-}]+[^{34}SO_4^{2-}] \tag{A2.7}$$

The terms ^{33}F and ^{34}F refer to the ratio of the species [$^{33}SO_4^{2-}$] and [$^{34}SO_4^{2-}$] with respect to [$^{32}SO_4^{2-}$], with $^{33}R_{std}$ = 0.00787726, and $^{34}R_{std}$ = 0.04416264 referring to the natural abundance ratios for our standards (Coplen and others, 2002).

$${}^{33}F=\frac{[^{33}SO_4^{2-}]}{[^{32}SO_4^{2-}]}=\left[\frac{\delta^{33}S_{SO_4}}{1000}+1\right]\cdot{}^{33}\Re_{std} \tag{A2.8}$$

$${}^{34}F=\frac{[^{34}SO_4^{2-}]}{[^{32}SO_4^{2-}]}=\left[\frac{\delta^{34}S_{SO_4}}{1000}+1\right]\cdot{}^{34}\Re_{std} \tag{A2.9}$$

$$\frac{{}^{33}F}{{}^{34}F}=\frac{[^{34}SO_4^{2-}]}{[^{33}SO_4^{2-}]} \tag{A2.10}$$

Equations A2.8-A2.10, in combination with A1.1 can be used to calculate the abundance/concentration of each of the species [$^{32}SO_4^{2-}$], [$^{33}SO_4^{2-}$], and [$^{34}SO_4^{2-}$], with respect to the bulk SO_4^{2-} concentration at the upper boundary condition, by algebraic manipulation, for [$^{32}SO_4^{2-}$]:

$$[SO_4^{2-}]=[^{32}SO_4^{2-}]+[^{32}SO_4^{2-}]{}^{33}F+[^{32}SO_4^{2-}]{}^{34}F=[^{32}SO_4^{2-}](1+{}^{33}F+{}^{34}F) \tag{A2.11}$$

$$[^{32}SO_4^{2-}]=[SO_4^{2-}]\left[\frac{1}{1+{}^{33}F+{}^{34}F}\right] \tag{A2.12}$$

And for [$^{33}SO_4^{2-}$]:

$$[SO_4^{2-}]=\frac{[^{33}SO_4^{2-}]}{{}^{33}F}+[^{33}SO_4^{2-}]+\frac{[^{33}SO_4^{2-}]\,{}^{34}F}{{}^{33}F}=[^{33}SO_4^{2-}]\left(\frac{1}{{}^{33}F}+1+\frac{{}^{34}F}{{}^{33}F}\right) \tag{A2.13}$$

$$[^{33}SO_4^{2-}]=[SO_4^{2-}]\left[\frac{1}{{}^{33}F}+1+\frac{{}^{34}F}{{}^{33}F}\right]^{-1}=[SO_4^{2-}]\left[\frac{{}^{33}F}{1+{}^{33}F+{}^{34}F}\right] \tag{A2.14}$$

And finally for [$^{34}SO_4^{2-}$]:

$$[SO_4^{2-}]=\frac{[^{34}SO_4^{2-}]}{{}^{34}F}+[^{34}SO_4^{2-}]\frac{{}^{33}F}{{}^{34}F}+[^{34}SO_4^{2-}]=[^{34}SO_4^{2-}]\left[\frac{1}{{}^{34}F}+\frac{{}^{33}F}{{}^{34}F}+1\right] \tag{A2.15}$$

$$[^{32}SO_4^{2-}]=[SO_4^{2-}]\left[\frac{1}{{}^{34}F}+\frac{{}^{33}F}{{}^{34}F}+1\right]^{-1}=[SO_4^{2-}]\left[\frac{{}^{34}F}{1+{}^{33}F+{}^{34}F}\right] \tag{A2.16}$$

In principle, this method can be used to derive the concentrations of the individual species anywhere within the domain of the reaction transport model, but only truly serves where the isotope ratios ($\delta^{34}S_{SO4}$, $\delta^{33}S_{SO4}$

and $\Delta^{33}S_{SO4}$) are satisfactorily known. The isotope model computes the concentrations of the species independently, but they are linked through the reaction terms ^{32}SRR, ^{33}SRR, and ^{34}SRR, which depend upon the constitutive fractionation factors ($^{33}\alpha_{SR}$ and $^{34}\alpha_{SR}$, linked by $^{33}\lambda_{SR}$). The derivation of these isotope-dependent rate terms is shown in the following section.

Lower Boundary Conditions for [$^{32}SO_4^{2-}$], [$^{33}SO_4^{2-}$], and [$^{34}SO_4^{2-}$]

In principal, it is possible to prescribe the lower boundary conditions for the species [$^{32}SO_4^{2-}$], [$^{33}SO_4^{2-}$], and [$^{34}SO_4^{2-}$] using isotope values, and thereby concentrations. However, such an approach is not possible, because the isotopic composition of sulfate is unknown at depth. In all cases, the model is run with Neumann boundary conditions, such that the isotopic composition is unchanging at depth, but without a specified composition:

$$\frac{d[^{32}SO_4^{2-}]_{x=L}}{dx} = 0, \quad \frac{d[^{33}SO_4^{2-}]_{x=L}}{dx} = 0, \quad \frac{d[^{34}SO_4^{2-}]_{x=L}}{dx} = 0 \tag{A2.17}$$

APPENDIX 3

TABLE A3

Pore water data from Berelson and others (2005) and isotope data generated in this study

Multicore ID	Depth (cm)	porosity (φ)	$[SO_4^{2-}]$ (mM)	DIC (mM)	Ca^{2+} (mM)	Depth CH_4 (cm)	$[CH_4]$ (mM)	$\delta^{34}S_{SO4}$ (SO_2) (‰)	$\delta^{34}S_{SO4}$ (SF_6) (‰)	$\Delta^{3}S_{SO4}$ (SF_6) (‰)
MC1	1	0.93	27.1	3.661	9.7	1	0.00047	21.7	21.9	0.0476
MC2	9.25	0.93	26.65	4.543	9.83	6.5	0.00138	22.7	21.9	0.0506
MC3	14.75	0.92	26.19	5.568	9.47	12	0.002225	23.9	24.0	0.0471
MC4	20.25	0.91	23.94	6.562	9.14	17.5	0.00278	25.7	25.6	0.0677
MC5	25.75	0.91	23.26	7.558	8.8	23	0.00376	26.6	27.0	0.0684
MC6	31.25	0.9	23.48	8.321	-	28.5	0.004625	-	-	-
MC7	36.75	0.89	23.03	9.449	8.12	34	0.005035	29.2	-	-
MC8	42.25	0.89	21.9	10.485	7.78	39.5	0.00647	31.5	30.5	0.0770
MC9	47.75	0.88	23.48	11.748	7.62	45	0.00689	33	33.0	0.0890

Gravity Core ID	Depth (cm)	porosity (φ)	$[SO_4^{2-}]$ (mM	DIC (mM)	Ca^{2+} (mM)	Depth CH_4 (cm)	$[CH_4]$ (mM)	$\delta^{34}S_{SO4}$ (SO_2) (‰)	$\delta^{34}S_{SO4}$ (SF_6) (‰)	$\Delta^{33}S_{SO4}$ (SF_6) (‰)
GC1	33	0.9	22.58	8.767	8.36	34.5	0.00501	-	29.6	0.0738
GC2	70	0.87	16.03	20.9	6.45	73.5	0.0152	-	-	-
GC3	113	0.85	10.84	30.08	5.33	114.5	0.0222	-	-	-
GC4	155	0.84	4.29	42.76	4.21	156.5	0.0873	-	-	-
GC5	193	0.83	3.16	39.99	3.69	194.5	1.172	-	-	
GC6	234	0.83	1.35	45.22	3.76	235.5	1.950	-	-	-
GC7	273	0.83	2.26	47.75	3.46	274.5	4.235	-	-	-

MCx reflects the Multicore.

Pore water geochemical and isotopic data from Alfonso Basin (CalMex Station 15) used in this study. Core samples were retrieved in October and November of 2001 during the California-Mexico margin (CalMex) cruise. Multi-cores (MC) and gravity cores (GC) were retrieved. Shallow multi-core (0-50 cm) MC1-MC9 were sectioned at higher intervals than deeper gravity core (GC1-GC7) samples. With the exception of the isotope data, all geochemical data were reported previously in Berelson and others (2005). Data missing here either had an error in sampling, or there was insufficient material for measurements.

REFERENCES

Aller, R. C., 2014, Sedimentary Diagenesis, Depositional Environments, and Benthic Fluxes: Treatise on Geochemistry, second edition, v. 8, p. 293–334, https://doi.org/10.1016/B978-0-08-095975-7.00611-2

Aller, R. C., and Blair, N. E., 1996, Sulfur diagenesis and burial on the Amazon shelf: Major control by physical sedimentation processes: Geo-Marine Letters, v. 16, n. 1, p. 3–10, https://doi.org/10.1007/BF01218830

Aller, R. C., Madrid, V., Chistoserdov, A., Aller, J. Y., and Heilbrun, C., 2010, Unsteady diagenetic processes and sulfur biogeochemistry in tropical deltaic muds: Implications for oceanic isotope cycles and the sedimentary record: Geochimica et Cosmochimica Acta, v. 74, n. 16, p. 4671–4692, https://doi.org/10.1016/j.gca.2010.05.008

Alperin, M. J., and Hoehler, T. M., 2009, Anaerobic methane oxidation by archaea/sulfate-reducing bacteria aggregates: 2. Isotopic constraints: American Journal of Science, v. 309, n. 10, p. 958–984, https://doi.org/10.2475/10.2009.02

Alperin, M. J., Albert, D. B., and Martens, C. S., 1994, Seasonal variations in production and consumption rates of dissolved organic carbon in an organic-rich coastal sediment: Geochimica et Cosmochimica Acta, v. 58, n. 22, p. 4909–4930, https://doi.org/10.1016/0016-7037(94)90221-6

Alperin, M. J., Martens, C. S., Albert, D. B., Suayah, I. B., Benninger, L. K., Blair, N. E., and Jahnke, R. A., 1999, Benthic fluxes and porewater concentration profiles of dissolved organic carbon in sediments from the North Carolina continental slope: Geochimica et Cosmochimica Acta, v. 63, n. 3–4, p. 427–448, https://doi.org/10.1016/S0016-7037(99)00032-0

Arndt, S., Jørgensen, B. B., LaRowe, D. E., Middelburg, J. J., Pancost, R. D., and Regnier, P., 2013, Quantifying the degradation of organic matter in marine sediments: A review and synthesis: Earth-Science Reviews, v. 123, p. 53–86, https://doi.org/10.1016/j.earscirev.2013.02.008

Bak, F., and Cypionka, H., 1987, A novel type of energy metabolism involving fermentation of inorganic sulphur compounds: Nature, v. 326, p. 891–892, https://doi.org/10.1038/326891a0

Bak, F., and Pfennig, N., 1987, Chemolithotrophic growth of desulfovibrio-sulfiodismutans sp-nov by disproportionation of inorganic sulfur-compounds: Archives of Microbiology, v. 147, n. 2, p. 184–189, https://doi.org/10.1007/BF00415282

Berelson, W. M., Prokopenko, M., Sansone, F. J., Graham, A. W., McManus, J., and Bernhard, J. M., 2005, Anaerobic diagenesis of silica and carbon in continental margin sediments: Discrete zones of TCO_2 production: Geochimica et Cosmochimica Acta, v. 69, n. 19, p. 4611–4629, https://doi.org/10.1016/j.gca.2005.05.011

Berner, R. A., 1964, An idealized model of dissolved sulfate distribution in recent sediments: Geochimica et Cosmochimica Acta, v. 28, n. 9, p. 1497–1503, https://doi.org/10.1016/0016-7037(64)90164-4

——— 1978, Sulfate reduction and the rate of deposition of marine sediments: Earth and Planetary Science Letters, v. 37, n. 3, p. 492–498, https://doi.org/10.1016/0012-821X(78)90065-1

——— 1980, Early Diagenesis-A Theoretical Approach: Princeton, New Jersey, Princeton University Press, 256 p.

Bigeleisen, J., and Mayer, M. G., 1947, Calculation of Equilibrium Constants for Isotopic Exchange Reactions: The Journal of Chemical Physics, v. 15, n. 5, p. 261–267, https://doi.org/10.1063/1.1746492

Boudreau, B. P., 1997, Diagenetic Models and Their Implementation: Berlin, Springer, 436 p.

Boudreau, B. P., and Westrich, J. T., 1984, The dependence of bacterial sulfate reduction on sulfate concentration in marine sediments: Geochimica et Cosmochimica Acta, v. 48, n. 12, p. 2503–2516, https://doi.org/10.1016/0016-7037(84)90301-6

Bowles, M. W., Mogollón, J. M., Kasten, S., Zabel, M., and Hinrichs, K. U., 2014, Global rates of marine sulfate reduction and implications for sub-sea-floor metabolic activities: Science, v. 344, n. 6186, p. 889–891, https://doi.org/10.1126/science.1249213

Bradley, A. S., Leavitt, W. D., Schmidt, M., Knoll, A. H., Girguis, P. R., and Johnston, D. T., 2016, Patterns of sulfur isotope fractionation during Microbial Sulfate Reduction: Geobiology, v. 14, n. 1, p. 91–101, https://doi.org/10.1111/gbi.12149

Brunner, B., and Bernasconi, S. M., 2005, A revised isotope fractionation model for dissimilatory sulfate reduction in sulfate reducing bacteria: Geochimica et Cosmochimica Acta, v. 69, n. 20, p. 4759–4771, https://doi.org/10.1016/j.gca.2005.04.015

Canfield, D. E., 2001, Biogeochemistry of sulfur isotopes: Reviews in Mineralogy and Geochemistry, v. 43, p. 607–636, https://doi.org/10.2138/gsrmg.43.1.607

——— 2004, The evolution of the Earth surface sulfur reservoir: American Journal of Science, v. 304, n. 10, p. 839–861, https://doi.org/10.2475/ajs.304.10.839

Canfield, D. E., and Farquhar, J., 2009, Animal evolution, bioturbation, and the sulfate concentration of the oceans: Proceedings of the National Academy of Sciences of the United States of America, v. 106, n. 20, p. 8123–8127, https://doi.org/10.1073/pnas.0902037106

Canfield, D. E., and Teske, A., 1996, Late Proterozoic rise in atmospheric oxygen concentration inferred from phylogenetic and sulphur-isotope studies: Nature, v. 382, p. 127–132, https://doi.org/10.1038/382127a0

Canfield, D. E., Farquhar, J., and Zerkle, A. L., 2010, High isotope fractionations during sulfate reduction in a low-sulfate euxinic ocean analog: Geology, v. 38, n. 5, p. 415–418, https://doi.org/10.1130/G30723.1

Coplen, T. B., Hopple, J. A., Boehike, J. K., Peiser, H. S., Rieder, S. E., Krouse, H. R., Rosman, K. J. R., Ding, T., Vocke, R. D., Jr., Révész, K. M., Lamberty, A., Taylor, P., and De Bièvre, P., 2002, Compilation of minimum and maximum isotope ratios of selected elements in naturally occurring terrestrial materials and reagents: U. S. Geological Survey, Water Resources Investigation Report 01-4222.

Dale, A. W., Brüchert, V., Alperin, M., and Regnier, P., 2009, An integrated sulfur isotope model for

Namibian shelf sediments: Geochimica et Cosmochimica Acta, v. 73, n. 7, p. 1924–1944, https://doi.org/10.1016/j.gca.2008.12.015
Detmers, J., Brüchert, V., Habicht, K. S., and Kuever, J., 2001, Diversity of sulfur isotope fractionations by sulfate-reducing prokaryotes: Applied and Environmental Microbiology, v. 67, n. 2, p. 888–894, https://doi.org/10.1128/AEM.67.2.888-894.2001
Donahue, M. A., Werne, J. P., Meile, C., and Lyons, T. W., 2008, Modeling sulfur isotope fractionation and differential diffusion during sulfate reduction in sediments of the Cariaco Basin: Geochimica et Cosmochimica Acta, v. 72, n. 9, p. 2287–2297, https://doi.org/10.1016/j.gca.2008.02.020
Farquhar, J., Johnston, D. T., Wing, B. A., Habicht, K. S., Canfield, D. E., Airieau, S., and Thiemens, M. H., 2003, Multiple sulphur isotopic interpretations of biosynthetic pathways: Implications for biological signatures in the sulphur isotope record: Geobiology, v. 1, n. 1, p. 27–36, https://doi.org/10.1046/j.1472-4669.2003.00007.x
Farquhar, J., Canfield, D. E., Masterson, A., Bao, H., and Johnston, D., 2008, Sulfur and oxygen isotope study of sulfate reduction in experiments with natural populations from Fællestrand, Denmark: Geochimica et Cosmochimica Acta, v. 72, n. 12, p. 2805–2821, https://doi.org/10.1016/j.gca.2008.03.013
Finster, K., Liesack, W., and Tindall, B. J., 1997, *Desulfospira joegensenii*, gen. nov. sp. nov, a new sulfate-reduing bacterium isolated from marine surface sediment: Systematic and Applied Microbiology, v. 20, n. 2, p. 201–208, https://doi.org/10.1016/S0723-2020(97)80066-5
Finster, K., Liesack, W., and Thamdrup, B., 1998, Elemental sulfur and thiosulfate disproportionation by *Desulfocapsa sulfoexigens* sp. nov., a new anaerobic bacterium isolated from marine surface sediment: Applied and Environmental Microbiology, v. 64, n. 1, p. 119–125.
Forrest, J., and Newman, L., 1977, Silver-110 microgram sulfate analysis for the short time resolution of ambient levels of sulfur aerosol: Analytical Chemistry, v. 49, n. 11, p. 1579–1584, https://doi.org/10.1021/ac50019a030
Goldhaber, M. B., and Kaplan, I. R., 1980, Mechanisms of sulfur incorporation and isotope fractionation during early diagenesis in sediments of the Gulf of California: Marine Chemistry, v. 9, n. 2, p. 95–143, https://doi.org/10.1016/0304-4203(80)90063-8
Gomes, M. L., and Hurtgen, M. T., 2013, Sulfur isotope systematics of a euxinic, low-sulfate lake: Evaluating the importance of the reservoir effect in modern and ancient oceans: Geology, v. 41, n. 6, p. 663–666, https://doi.org/10.1130/G34187.1
Gonzalez-Yajimovich, O. E., ms, 2004, Holocene sedimentation in the Gulf of California and its Climatic implications: Los Angeles, California, University of Southern California, Ph. D. thesis, 211 p.
Gonzalez-Yajimovich, O. E., Gorsline, D. S., and Douglas, R. G., 2007, Frequency and sources of basin floor turbidites in Alfonso Basin, Gulf of California, Mexico: Products of slope failures: Sedimentary Geology, v. 199, n. 1–2, p. 91–105, https://doi.org/10.1016/j.sedgeo.2005.09.025
Habicht, K. S., and Canfield, D. E., 2001, Isotope fractionation by sulfate-reducing natural populations and the isotopic composition of sulfide in marine sediments: Geology, v. 29, n. 6, p. 555–558, https://doi.org/10.1130/0091-7613(2001)029<0555:IFBSRN>2.0.CO;2
——— 1997, Sulfur isotope fractionation during bacterial sulfate reduction in organic-rich sediments: Geochimica et Cosmochimica Acta, v. 61, n. 24, p. 5351–5361, https://doi.org/10.1016/S0016-7037(97)00311-6
Habicht, K. S., Canfield, D. E., and Rethmeier, J. O., 1998, Sulfur isotope fractionation during bacterial reduction and disproportionation of thiosulfate and sulfite: Geochimica et Cosmochimica Acta, v. 62, n. 15, p. 2585–2595, https://doi.org/10.1016/S0016-7037(98)00167-7
Habicht, K. S., Gade, M., Thamdrup, B., Berg, P., and Canfield, D. E., 2002, Calibration of sulfate levels in the Archean ocean: Science, v. 298, n. 5602, p. 2372–2374, https://doi.org/10.1126/science.1078265
Johnston, D. T., 2011, Multiple sulfur isotopes and the evolution of Earth's surface sulfur cycle: Earth-Science Reviews, v. 106, n. 1–2, p. 161–183, https://doi.org/10.1016/j.earscirev.2011.02.003
Johnston, D. T., Farquhar, J., Wing, B. A., Kaufman, A. J., Canfield, D. E., and Habicht, K. S., 2005a, Multiple sulfur isotope fractionations in biological systems: A case study with sulfate reducers and sulfur disproportionators: American Journal of Science, v. 305, n. 6–8, p. 645–660, https://doi.org/10.2475/ajs.305.6-8.645
Johnston, D. T., Wing, B. A., Farquhar, J., Kaufman, A. J., Strauss, H., Lyons, T. W., Kah, L. C., and Canfield, D. E., 2005b, Active microbial sulfur disproportionation in the Mesoproterozoic: Science, v. 310, n. 5753, p. 1477–1479, https://doi.org/10.1126/science.1117824
Johnston, D. T., Farquhar, J., and Canfield, D. E., 2007, Sulfur isotope insights into microbial sulfate reduction: *When microbes meet models*: Geochimica et Cosmochimica Acta, v. 71, n. 16, p. 3929–3947, https://doi.org/10.1016/j.gca.2007.05.008
Johnston, D. T., Farquhar, J., Habicht, K. S., and Canfield, D. E., 2008, Sulphur isotopes and the search for life: Strategies for identifying sulphur metabolisms in the rock record and beyond: Geobiology, v. 6, n. 5, p. 425–435, https://doi.org/10.1111/j.1472-4669.2008.00171.x
Johnston, D. T., Gill, B. C., Masterson, A., Beirne, E., Casciotti, K. L., Knapp, A. N., and Berelson W., 2014, Placing an upper limit on cryptic marine sulphur cycling: Nature, v. 513, n. 7519, 530–533, https://doi.org/10.1038/nature13698
Jorgensen, B. B., 1979, A theoretical model of the stable sulfur isotope distribution in marine sediments: Geochimica et Cosmochimica Acta, v. 43, n. 3, p. 363–374, https://doi.org/10.1016/0016-7037(79)90201-1
——— 1982, Mineralization of organic matter in the sea bed: The role of sulphate reduction: Nature, v. 296, p. 643–645, https://doi.org/10.1038/296643a0
Kemp, A. L. W., and Thode, H. G., 1968, The mechanism of the bacterial reduction of sulphate and of sulphite from isotope fractionation studies: Geochimica et Cosmochimica Acta, v. 32, n. 1, p. 71–91, https://doi.org/10.1016/0016-7037(68)90088-4

Leavitt, W. D., Halevy, I., Bradley, A. S., and Johnston, D. T., 2013, Influence of sulfate reduction rates on the Phanerozoic sulfur isotope record: Proceedings of the National Academy of Sciencs of the United States of America, v. 110, n. 28, p. 11244–11249, https://doi.org/10.1073/pnas.1218874110

Leavitt, W. D., Bradley, A. S., Santos, A. A., Pereira, I. A., and Johnston, D. T., 2015, Sulfur Isotope Effects of Dissimilatory Sulfite Reductase: Frontiers in Microbiology, v. 6, 1392, https://doi.org/10.3389/fmicb.2015.01392

Li, Y-H., and Gregory, S., 1974, Diffusion of ions in sea water and in deep-sea sediments: Geochimica et Cosmochimica Acta, v. 38, n. 5, p. 703–714, https://doi.org/10.1016/0016-7037(74)90145-8

Masterson, A. L., Wing, B. A., Paytan, A., Farquhar, J., and Johnston, D. T., 2016, The minor sulfur isotope composition of Cretaceous and Cenozoic seawater sulfate: Paleoceanography and Paleoclimatology, v. 31, n. 6, p. 779–788, https://doi.org/10.1002/2016PA002945

Niewöhner, C., Hensen, C., Kasten, S., Zabel, M., and Schulz, H. D., 1998, Deep sulfate reduction completely mediated by anaerobic methane oxidation in sediments of the upwelling area off Namibia: Geochimica et Cosmochimica Acta, v. 62, n. 3, p. 455–464, https://doi.org/10.1016/S0016-7037(98)00055-6

Ono, S., Wing, B., Johnston, D., Farquhar, J., and Rumble, D., 2006, Mass-dependent fractionation of quadruple stable sulfur isotope system as a new tracer of sulfur biogeochemical cycles: Geochimica et Cosmochimica Acta, v. 70, n. 9, p. 2238–2252, https://doi.org/10.1016/j.gca.2006.01.022

Parkes, R. J., Cragg, B., Roussel, E., Webster, G., Weightman, A., and Sass, H., 2014, A review of prokaryotic populations and processes in sub-seafloor sediments, including biosphere: Geosphere interactions: Marine Geology, v. 352, p. 409–425, https://doi.org/10.1016/j.margeo.2014.02.009

Peck, H. D., Jr., 1961, Evidence for the reversibility of the reaction catalyzed by adenosine 5 -phosphosulfate reductase: Biochimica et Biophysica Acta, v. 49, n. 3, p. 621–624, https://doi.org/10.1016/0006-3002(61)90273-6

——— 1959, The ATP-dependent reduction of sulfate with hydrogen in extracts of Desulfovibrio desulfuricans; Proceedings of the National Academy of Sciences of the United States of America, v. 45, n. 5, p. 701–708, https://doi.org/10.1073/pnas.45.5.701

Pellerin, A., Bui, T. H., Rough, M., Mucci, A., Canfield, D. E., and Wing, B. A., 2015, Mass-dependent sulfur isotope fractionation during reoxidative sulfur cycling: A case study from Mangrove Lake, Bermuda: Geochimica et Cosmochimica Acta, v. 149, p. 152–164, https://doi.org/10.1016/j.gca.2014.11.007

Rees, C. E., 1973, A steady-state model for sulphur isotope fractionation in bacterial reduction processes: Geochimica et Cosmochimica Acta, v. 37, n. 5, p. 1141–1162, https://doi.org/10.1016/0016-7037(73)90052-5

Reimers, C. E., Ruttenberg, K. C., Canfield, D. E., Christiansen, M. B., and Martin, J. B., 1996, Porewater pH and authigenic phases formed in the uppermost sediments of the Santa Barbara Basin: Geochimica et Cosmochimica Acta, v. 60, n. 21, p. 4037–4057, https://doi.org/10.1016/S0016-7037(96)00231-1

Sansone, F. J., Graham, A. W., and Berelson, W. M., 2004, Methane along the western Mexican margin: Limnology and Oceanography, v. 49, n. 6, p. 2242–2255, https://doi.org/10.4319/lo.2004.49.6.2242

Silverberg, N., Aguirre-Bahena, F., and Mucci, A., 2014, Time-series measurements of settling particulate matter in Alfonso Basin, La Paz Bay, southwestern Gulf of California: Continental Shelf Research, v. 84, p. 169–187.

Sim, M. S., Bosak, T., and Ono, S., 2011, Large sulfur isotope fractionation does not require disproportionation: Science, v. 333, n. 6038, p. 74–77, https://doi.org/10.1126/science.1205103

Sim, M. S., Ono, S., and Bosak, T., 2012, Effects of iron and nitrogen limitation on sulfur isotope fractionation during microbial sulfate reduction: Applied and Environmental Microbiology, v. 78, n. 23, p. 8368–8376, https://doi.org/10.1128/AEM.01842-12

Staines-Urías, F., González-Yajimovich, O., and Beaufort, L., 2015, Reconstruction of past climate variability and ENSO-like fluctuations in the southern Gulf of California (Alfonso Basin) since the last glacial maximum: Quaternary Research, v. 83, n. 3, p. 488–501, https://doi.org/10.1016/j.yqres.2015.03.007

Strauss, H., 1999, Geological evolution from isotope proxy signals?sulfur: Chemical Geology, v. 161, n. 1–3, p. 89–101, https://doi.org/10.1016/S0009-2541(99)00082-0

Tarpgaard, I. H., Røy, H., and Jørgensen, B. B., 2011, Concurrent low- and high-affinity sulfate reduction kinetics in marine sediment: Geochimica et Cosmochimica Acta, v. 75, n. 11, p. 2997–3010, https://doi.org/10.1016/j.gca.2011.03.028

Thamdrup, B., Finster, K., Hansen, J. W., and Bak, F., 1993, Bacterial disproportionation of elemental sulfur coupled to chemical reduction of iron or manganese: Applied and Environmental Microbiology, v. 59, n. 1, p. 101–108.

Thamdrup, B., Fossing, H., and Jorgensen, B. B., 1994, Manganese, iron, and sulfur cycling in a coastal marine sediment, Aarhus Bay, Denmark: Geochimica et Cosmochimica Acta, v. 58, n. 23, p. 5115–5129, https://doi.org/10.1016/0016-7037(94)90298-4 10.1016/0016-7037(94)90298-4

Ullman, W. J., and Aller, R. C., 1982, Diffusion coefficients in nearshore marine sediments: Limnology and Oceanography, v. 27, n. 3, p. 552–556, https://doi.org/10.4319/lo.1982.27.3.0552

Westrich, J. T., and Berner, R. A., 1984, The role of sedimentary organic matter in bacterial sulfate reduction: The *G* model tested: Limnology and Oceanography, v. 29, n. 2, p. 236–249, https://doi.org/10.4319/lo.1984.29.2.0236

Wing, B. A., and Halvey, I., 2014, Intracellular metabolite levels shape sulfur isotope fractionation during microbial sulfate respiration: Proceedings of the National Academy of the United States of America, v. 111, n. 51, p. 18116–18125, https://doi.org/10.1073/pnas.1407502111

Wortmann, U. G., Bernasconi, S. M., and Böttcher, M. E., 2001, Hypersulfidic deep biosphere indicates extreme sulfur isotope fractionation during single-step microbial sulfate reduction: Geology, v. 29, n. 7, p. 647–650, https://doi.org/10.1130/0091-7613(2001)029<0647:HDBIES>2.0.CO;2

Wu, N., Farquhar, J., Strauss, H., Kim, S.-T., and Canfield, D. E., 2010, Evaluating the S-isotope fractionation

associated with Phanerozoic pyrite burial: Geochimica et Cosmochimica Acta, v. 74, n. 7, p. 2053–2071, https://doi.org/10.1016/j.gca.2009.12.012

Wu, N., Farquhar, J., and Fike, D. A., 2015, Ediacaran sulfur cycle: Insights from sulfur isotope measurements ($\Delta^{33}S$ and $\delta^{34}S$) on paired sulfate–pyrite in the Huqf Supergroup of Oman: Geochimica et Cosmochimica Acta, v. 164, p. 352–364, https://doi.org/10.1016/j.gca.2015.05.031

Young, E. D., Galy, A., and Nagahara, H., 2002, Kinetic and equilibrium mass-dependent isotope fractionation laws in nature and their geochemical and cosmochemical significance: Geochimica et Cosmochimica Acta, v. 66, n. 6, p. 1095–1104, https://doi.org/10.1016/S0016-7037(01)00832-8

Zeebe, R. E., and Wolf-Gladrow, D., 2001, CO_2 in Seawater: Elsevier Oceanography Series, Equilibrium, Kinetics, Isotopes, v. 65, 360 p.